The Thesis Committee for Konstantinos Iliopoulos
Certifies that this is the approved version of the following Thesis:

VISVE, a Vorticity Based Model Applied to 2-D Hydrofoils in Cavitating Conditions

APPROVED BY
SUPERVISING COMMITTEE:

Spyridon A. Kinnas, Supervisor

Laxminarayan Raja

VISVE, a Vorticity Based Model Applied to 2-D Hydrofoils in Cavitating Conditions

by

Konstantinos Iliopoulos

Thesis

Presented to the Faculty of the Graduate School of

The University of Texas at Austin

in Partial Fulfillment

of the Requirements

for the Degree of

MASTER OF SCIENCE IN ENGINEERING

The University of Texas at Austin

August 2020

Dedication

Dedicated to my family for their love and support.

Acknowledgements

I would like to acknowledge the invaluable support from the following professors, colleagues and friends. I appreciate the time and effort they have contributed to help me during my study at the Ocean Engineering Group of the Department of Civil Architectural and Environmental Engineering.

I would like to first express my deep gratitude to my supervisor, Professor Spyridon Kinnas, for his guidance and support on my work. I would also like to acknowledge the patience and trust he showed me during the more difficult parts of this project.

I would also like to recognize my second reader, Professor Laxminarayan Raja for his interest in my research. I appreciate him for all the deep thoughts and constructive comments.

In addition, I would acknowledge the invaluable support from my colleagues at the Ocean Engineering Group. First, I would like to dedicate my special thanks to Lu Xing who laid the foundation for this work. I would also like thank to Dr. Weikang Du, Chunlin Wu and Seungnam Kim who were willing to offer their help and support.

Finally, I am grateful to my parents Dimitrios Iliopoulos and Christine Pitta for their utmost love and endless support through all my personal endeavors.

Support for this research was provided by the U.S. Office of Naval Research (Grant Nos. N00014-14-1-0303 and N00014-18-1-2276; Dr. Ki-Han Kim) partly by Phase VIII of the “Consortium on Cavitation Performance of High Speed Propulsors”.

Abstract

VISVE, a Vorticity Based Model Applied to 2-D Hydrofoils in Cavitating Conditions

Konstantinos Iliopoulos, M.S.E.

The University of Texas at Austin, 2020

Supervisor: Spyridon A. Kinnas

In this study, the VIScous Vorticity Equation (VISVE) method was applied to predict flow around 2-D hydrofoils in cavitating conditions. The DIVergence of velocity Equation (DIVE) was added to extend the method to compressible flows and coupled with VISVE to predict the partial cavitating flow. The flow was modeled as a homogenous mixture of vapor and liquid with the vapor volume fraction parameter determining their concentrations inside the volume and an additional transport equation for the vapor volume fraction to predict the partial cavitating flow around 2-D hydrofoils. The VISVE method was designed to be both spatially compact and numerically efficient in comparison with the commonly used Reynolds Averaged Navier-Stokes (RANS) models.

Cavity shapes and pressure from the VISVE model were compared with those from a commercial RANS solver to assess the accuracy of the numerical results. With the validation of the 2-D VISVE model, VISVE shows the prospective to model the 3D wetted and cavitating flow.

Table of Contents

List of Tables

List of Figures

Nomenclature

A	Matrix of the system of equations
A_D	Diagonal of matrix A
A_{OD}	Off-diagonal of matrix A
$\tilde{A}_D$	Modified value of A_D (SIMPLE/SIMPLEC)
C	Evaporation/Condensation Constant
DIVE	DIVergence Equation
L	Length scale (length of the foil)
n	Bubble concentration per unit liquid
n_0	Bubble density (per unit volume)
P_ω	Baroclinic torque
$P_{\vec{\nabla}\cdot\vec{\mathrm{q}}}$	Pressure sources
p_∞	Pressure upstream
p	Local pressure
p_0	First approximation of pressure
p_{cor}	Pressure correction
p_v	Saturated vapor pressure
q	Proxy for pressure
$\vec{q}_\infty$	Velocity upstream
$\vec{q}_\omega$	Vorticity Induced velocity
$\vec{q}_{\vec{\nabla}\cdot\vec{q}}$	Sources/Sinks Induced Velocity
Q_ω	Residual Viscous terms in VISVE
$Q_{\vec{\nabla}\cdot\vec{q}}$	Residual Viscous terms in DIVE

R	Evaporation/Condensation Rate
$\Re_B$	Bubble Radius
$\bar{\bar{S}}$	Strain tensor
$\bar{\bar{T}}$	Stress tensor
U	Velocity scale (upstream velocity)
VISVE	VIScous Vorticity Equation
α	Vapor volume fraction
γ	Surface vorticity distribution
μ	Dynamic viscosity
ν	Kinematic viscosity
ξ	Velocity potential
ρ	Density
σ	Surface source/sinks distribution
ϕ	B.E.M velocity potential
$\vec{\psi}$	Stream function
ω	Vorticity

Chapter 1: Introduction

1.1 BACKGROUND

Over the past decades, the study of the cavitation phenomenon has become an integral part in the process of propeller design. Nowadays, the propeller is expected to operate reliably and efficiently under different conditions, including high loading and partial or full cavitation. At those off-design points issues of flow separation, noise, vibrations or even erosion arise requiring the careful study of flow around the propeller. Traditional potential flow methods have been successful in describing the cavitation phenomenon under normal operating conditions while offering a reasonable computational cost to accuracy solution. Their usage however is limited to certain types of cavitation and flow regimes. For example, at very high loading, the Boundary Element Methods (BEM) fail to capture flow separation which is a viscous driven phenomenon and as a result tend to overpredict the thrust and torque of the propellers. Additionally, BEM are designed to model sheet cavitation and cannot describe cloud or bubble type cavitation which may cause serious erosion.

The VIScous Vorticity Equation (VISVE) model was developed to address the problems of BEM at the off-design points. Specifically, VISVE method, first proposed and implemented by Tian and Kinnas [1], managed to successfully model the complex flow separation. Results comparing the leading-edge vortex predicted by VISVE and Reynold Averaged Navier-Stokes equation RANS are shown in figure 1.1. The method has already been extended in the case of 3-D hydrofoils by Wu *et al* [2,3] and propellers by Wu and Kinnas [4], as well as cylinders in unidirectional and alternating flow by Wu [5], Li and Kinnas [6, 7].

Moreover, VISVE was recently coupled with turbulence models (Open-FOAM) in the case of wetted flows past a 2-D hydrofoil by Hao and Kinnas [8], while Ms. You is currently working on embedding a turbulence model into VISVE. Additional turbulent results for 2-D hydrofoil as well as laminar flow results around a 3-D rectangular foil are presented by Wu and Kinnas in [9].

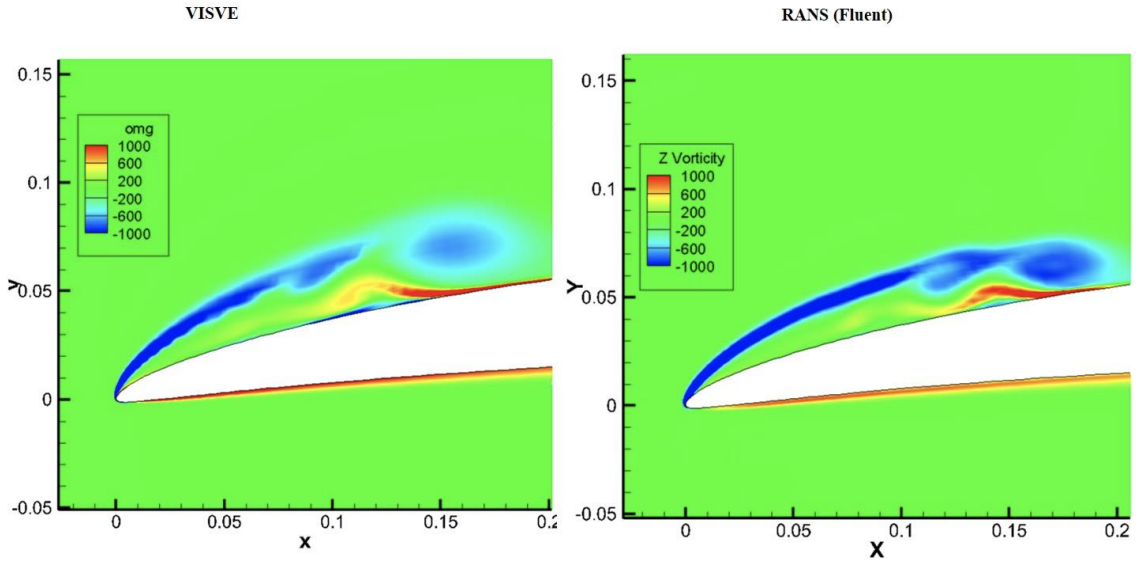

Figure 1.1: Leading edge vortex predicted by VISVE and RANS from Tian [10].

1.2 MOTIVATION

The VISVE model has been well validated in case of hydrofoils in forward and backing conditions, as well as in the case of turbulence flows. In the past there had been an attempt to include the cavitation model into the VISVE model by Xing [11] but the results were not satisfactory. Therefore, it is necessary to revisit the topic of cavitation and

improve upon the existing formulation in order to achieve a more reliable cavitation model for the VISVE solver.

1.3 OBJECTIVES

The objectives of this research are to apply the 2-D VISVE model to predict the flow around hydrofoils in cavitating conditions. Specifically, an additional equation governing the local expansion rate will be added, in order to address the compressible characteristics of the flow. The description of the homogeneous mixture of liquid and vapor near cavity is based on the Mixture Model which introduces the vapor volume fraction parameter and the accompanying vapor transport equation describing the evolution of the cavity in time. Cavitation models proposed by Schnerr *et al* [12] and Zwart *et al* [13] will be embedded in the solver. In this thesis, results from the model proposed by Zwart *et al* [13] will be presented.

1.4 OVERVIEW

This thesis is organized into five main chapters:

Chapter 1 contains background, motivation and objectives of this research.

Chapter 2 provides a brief literature review of vorticity methods, mixture models and cavitation models.

Chapter 3 presents the detailed mathematical formulation and numerical implementation of the VISVE method, the mixture model, and the coupling scheme between them.

Chapter 4 represents the results for two- dimensional hydrofoils in cavitating conditions. The results from VISVE are compared with those from a RANS-based commercial CFD software.

Chapter 5 summarizes the present work and proposes the recommendation for future VISVE related works.

Chapter 2: Literature Review

This chapter reviews the related literature on two topics: vortex-based methods and cavitation.

2.1 VORTEX METHOD

The vorticity formulations offer an alternate perspective when studying fluid phenomena, and in many cases it is advantageous to describe dynamic events in the flow in terms of the evolution of the vorticity field [14]. Vortex methods were initially proposed and developed to predict the hydrodynamic behavior of inviscid flow. The first dynamic vortex simulation may be traced back to 1930s [15] in the works of Rosenhead [16, 17], who calculated vortex sheet with the point vortex method. Numerical issues due to the singular behavior of the induced velocity near the point vortex led to the development of analytical solutions based on the Biot-Savart expression [18,19], in an effort to remove the singularity, and the vortex blob method [20]. During the early 1980s, the focus shifted to mathematical issues of the vortex methods such as their convergence properties [21, 22]. In the later years, the development of the vortex method has been very diverse, including but not limited to the generalization to viscous flow [23], the treatment of interior boundary conditions [24], the extension to high-Reynold number flow [25] and the improvement of computational efficiency [26]. Comprehensive reviews of the development of vortex method can be found in [15, 27].

In general, the vortex method is characterized by two major features. Firstly, the vorticity transport equation is formulated in terms of vorticity, so the computational domain focuses on the vorticity field instead of the velocity field. Secondly, the Biot- Savart law

can be applied to obtain the velocity field from the computed vorticity field. Then, the flow field can be completely described by tracking vorticity.

2.1.1 Advantages of Vortex Method

The predominant advantage of vortex method lies on the fact that compared with velocity, vorticity is a dimensionally compact variable. Specifically, in the case of a flow around a hydrofoil the vorticity is generated only at the wall, which implies that the vorticity is concentrated in a small area near the wall and the wake of the foil. The volume of fluid with a significant amount of vorticity is typically of a relatively small fraction. Therefore, a much smaller computational domain is required in order to describe the flow in terms of vorticity, which in turn improves the computational efficiency. Another advantage is the simplification of grid generating process. In VISVE, the computational grid can be generated automatically based on the discretization of the foil's surface. In addition, the boundary conditions at far field can be automatically satisfied by using Green's function.

In the special case of incompressible, constant- temperature, single-phase, 2-D flow there is only one governing equation describing the flow field. In particular, by taking the curl of the Navier-Stokes equations, the two momentum equations are replaced by the vorticity transport equation below, with the vorticity induced velocity satisfying the continuity equation.

$$\frac{\partial \omega}{\partial t} + \nabla \cdot (\vec{q}\omega) = \nabla(\nu \nabla \omega) \tag{2.1}$$

where, ω is the vorticity, $\vec{q}$ is the velocity, ν is the kinematic viscosity, t is the time. Unlike velocity-pressure formulation of Navier-Stokes equation, the above equation is now only dependent on vorticity and velocity. This formulation enjoys the absence of the pressure

terms, thus pressure evaluation is not coupled with the vorticity transport equation, instead, it is needed only when force measurements are desired.

In the case of compressible 2-D flows there is an additional governing equation describing the local expansion and compression rate, namely the DIVergence of velocity Equation (DIVE).

$$\frac{\partial(\vec{\nabla}\cdot\vec{q})}{\partial t}+\vec{\nabla}\cdot(\vec{q}\,\vec{\nabla}\cdot\vec{q})=\vec{\nabla}\left(\nu\vec{\nabla}(\vec{\nabla}\cdot\vec{q})\right)-\vec{\nabla}\cdot\left(\frac{\vec{\nabla}p}{\rho}\right)+Q_{\vec{\nabla}\cdot\vec{q}} \tag{2.2}$$

However, in the case of cavitating flows the compressible part of the flow is restricted close to the foil. Therefore, sources share similar attributes with vorticity in the case of cavitation.

2.1.2 Disadvantages of Vortex Method

Despite its simplicity and computational efficiency, the vortex method has not yet become a part of the mainstream computational tools for CFD. The main issue with VISVE (and DIVE) is the implementation of the inner boundary condition. Unlike RANS where the kinematic, no through, and viscous, no slip, boundary conditions can be expressed as Dirichlet boundary conditions for the momentum equations, the boundary condition for the vorticity is not as straightforward. In particular advancing the vorticity field to the next time-step using equation (2.1) does not guarantee that the vorticity induced velocity will be zero at the wall. The no through boundary condition can be satisfied by solving the corresponding BEM problem, creating a vorticity distribution on the surface of the foil. The issue now becomes, how this vorticity sheet enters the flow in order to satisfy the no-slip boundary condition. Under certain assumptions a Neumann or a Dirichlet boundary condition for the vorticity equation can be extracted from the value of the vortex sheet strength at any point on the foil [24] but there is still no widely accepted mathematical convergence proof for these methods. Cottet [15] and Anderson [27] computed the exact

vorticity boundary condition from different approaches. However, the resulting equations are equivalent to the original set of Navier-Stokes equation and the stability of those numerical algorithms is still not clearly understood.

2.2 CAVITATION

From a theoretical standpoint the cavitation phenomenon describes the rapid phase change between liquid and vapor. The main parameter of cavitation is the saturated vapor pressure p_v which is a function of temperature as can be seen in Figure 2.1. Specifically for a constant temperature mixture of liquid and vapor (in equilibrium), increasing the pressure over p_v leads to condensation of the vapor phase, while decreasing the pressure below p_v leads to evaporation of the liquid phase.

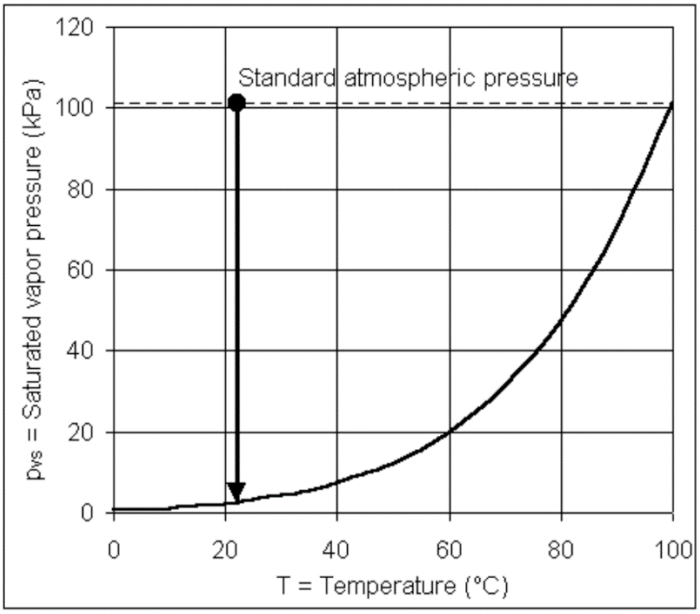

Figure 2.1: Saturated vapor pressure for water [28]

Figure 2.1 implies that changes in temperature under constant pressure may also cause the transition between vapor and liquid, which in this case is known as ebullition. For example, at standard atmospheric pressure water boils at 100 ^{o}C. In the mathematical formulation of chapter 3, however, the variations in temperature will be ignored.

In practice cavitation is a common phenomenon in hydrofoils, pipe flows, liquid pumps and marine propellers where there are significant pressure differentials. Depending on the application, cavitation can be the cause of several detrimental effects including structural failure, corrosion, vibration and noise radiation.

Cavitation plays a significant role in the propeller design process and over the years there has been a great effort in recognizing and categorizing the different types of cavitation. Figure 2.2 shows the types of propeller cavitation based on their location (tip vortex cavitation) and their appearance (bubble cavitation).

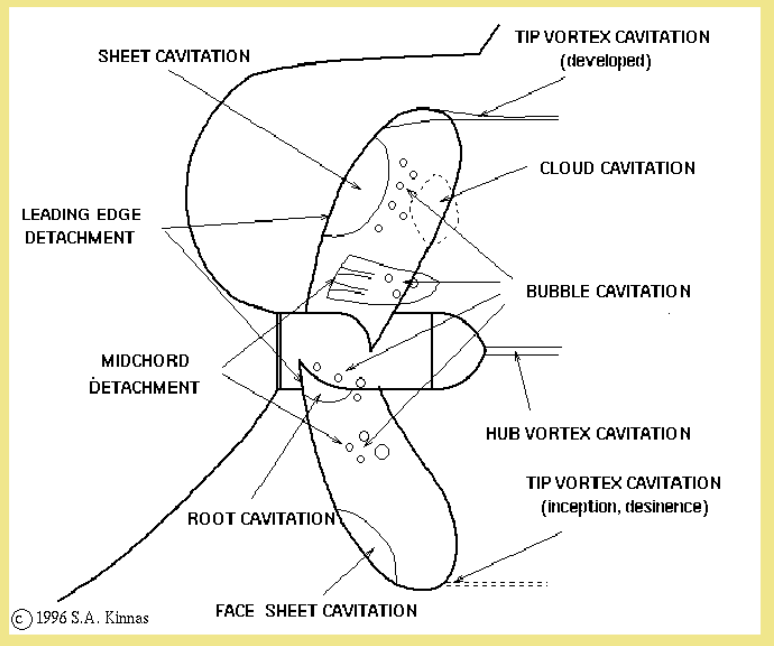

Figure 2.2: Types of propeller cavitation [28]

The focus of this thesis will be on the sheet cavitation which is defined as a thin, quasi-steady layer of vapor, occurring near leading edge where the pressure distribution has a strong adverse gradient. The cavity shape interface is partly attached to the solid surface, as shown in Figure 2.3.

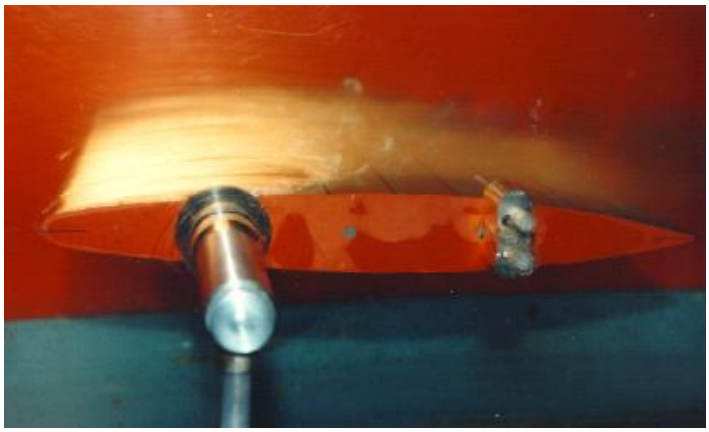

Figure 2.3: Sheet cavity around hydrofoil [28]

2.2.1 Cavitation Models

Over the past years, several models have been developed in an effort to describe and predict the cavitation phenomenon. Potential flow models treat the cavity as additional thickness to the hydrofoil where the kinematic no-through boundary condition needs to be satisfied [29] and are best suited for sheet cavitation. Viscous models, on the other hand, vary depending on the application but in general are spilt into four broad categories. Based on the treatment of the vapor phase, there are:

- Discrete Bubble Models

  These models track the evolution of a finite number of small bubbles inserted inside the liquid [30]. They focus on the effects the surrounding liquid has on growth and collapse of each individual bubble, while neglecting the effect of the bubble on the fluid. These models are suitable in the cases when cavitation inception is of great concern.

- Vapor Transport Models

  These models are best suited for large scale cavitation, like sheet and bubble cavitation. In this case the presence of the cavity directly affects the liquid phase with two-way interactions between the phases, governing the evaporation and condensation process.

In the case of two-phase cavitation, the models may also be distinguished by whether or not they keep track of the interphase:

- Sharp Interface Tracking Models

  The distinguishing feature of these models is that the interface is not diffused by advection, so that a sharp interphase between the phases is maintained. Interfaces are modeled by adding appropriate source term at the boundary to separate the two phases and maintain a clear and distinct interface [31]. This kind of methods is only appropriate when the cavity size can be assumed to be at least larger than the cell.

- Homogeneous Mixture Models

  Homogeneous mixture models make no attempt to track the interface, but regard the multiphase flow as one phase of an averaged mixture with homogenous physical properties [32]. Therefore, the contents of an individual cell are considered uniform, which is well suited to modeling large numbers of small bubbles.

2.2.2 Phase change Models

There are three general categories of phase change models used for cavitation, which are the barotropic models, equilibrium models and models derived from Rayleigh-Plesset equation.

- Barotropic Model

  In this type of models, it is assumed that if the pressure is greater than vapor pressure, the fluid is occupied by liquid, otherwise, vapor.

$$\rho = \begin{cases} \rho_v , & p < p_v \\ \rho_l , & p \geq p_v \end{cases} \tag{2.3}$$

  where, ρ_v , ρ_l represents the density of the vapor and liquid phase; p_v is the saturated vapor pressure at the given operating temperature. A smoothed function can be applied to deal with the stability issues. The major disadvantage of this method is that it cannot capture the baroclinic torque, $\frac{1}{\rho^2}\vec{\nabla}\rho \times \vec{\nabla}p$, due to the difference between the pressure and density gradients. [33]

- Equilibrium Model

  This method requires the solution of the energy equation for the water phase. The energy absorbed and released by phase change creates local temperature gradients which control the rate of change phase [34]. The disadvantage is mainly due to the

high computational cost and the fact that local temperature gradient is not the dominant factor for the phase change rate.

- Rayleigh- Plesset based Models

  In the past few decades, there are several phase change models developed based on Rayleigh-Plesset equation [35], as shown in equation (2.4):

$$\rho_l \left(\Re_B \ddot{\Re}_B + \frac{3}{2} \dot{\Re}_B^{\,2} \right) = p_v - p_\infty + p_{g0} \left(\frac{R_o}{\Re_B} \right)^{3\gamma} - \frac{2S}{\Re_B} - \frac{4\mu \dot{\Re}_B}{\Re_B} \qquad (2.4)$$

  where, $\Re_B$ is the bubble radius, p_∞ is the ambient pressure; p_{go} is the initial partial pressure for the non-condensable gasses; R_o is the initial radius of the bubbles; S is the surface tension. The third term on the right-hand side represents the effect of the non-condensable gasses. The last two terms on the right represent the effects of surface tension and viscosity, respectively. Different models in this category make different assumptions to simplify the Rayleigh-Plesset equation. The common aspects they share are that these models assume a bubble of saturated vapor growing in an infinite, viscous and incompressible medium and heat exchange is neglected. In this thesis, two models in this category were adopted to predict the cavitating flow around the two-dimensional hydrofoil. Detailed formulation of the models will be represented in Section 3.5.

Chapter 3: The VISVE / DIVE Method

The VIScous Vorticity Equation (VISVE), the DIVergence of velocity Equation (DIVE) and the homogeneous mixture model, which introduces an additional transport equation for the vapor volume fraction, were coupled together to predict the partial cavitating flow around a two-dimensional hydrofoil. The cavitation was modeled by Schnerr-Saucer's [12] and Zwart-Gerber-Belamri's [13] model. A pressure correction method, based on the SIMPLEC algorithm, was used to satisfy the continuity equation.

3.1 General Solving Algorithm

In this thesis, the original solving algorithm in VISVE model was modified to take the cavitating effects into consideration. The Divergence equation, along with vapor transport and continuity (in the form of pressure correction) equations were added, in order to model the compressible flow near the cavity. The general solving algorithm within a time step (n) is shown in Figure 3.1, where n presents the time increment. The blue blocks represent the process or solver. The red blocks show the corresponding outcomes from the upstream process or solver.

At each time step there are only three variables needed in order to fully describe the flow. The vapor volume fraction, α, describing the cavity, is needed for the calculation of mixture density, ρ, and dynamic viscosity, μ. Based on the vector field decomposition theorem, the velocity field can be broken down to a vorticity induce velocity field, $\vec{q}_{\omega}$, a source induced velocity field, $\vec{q}_{\nabla\cdot\vec{q}}$ and the far field velocity $\vec{q}_{\infty}$ which is constant.

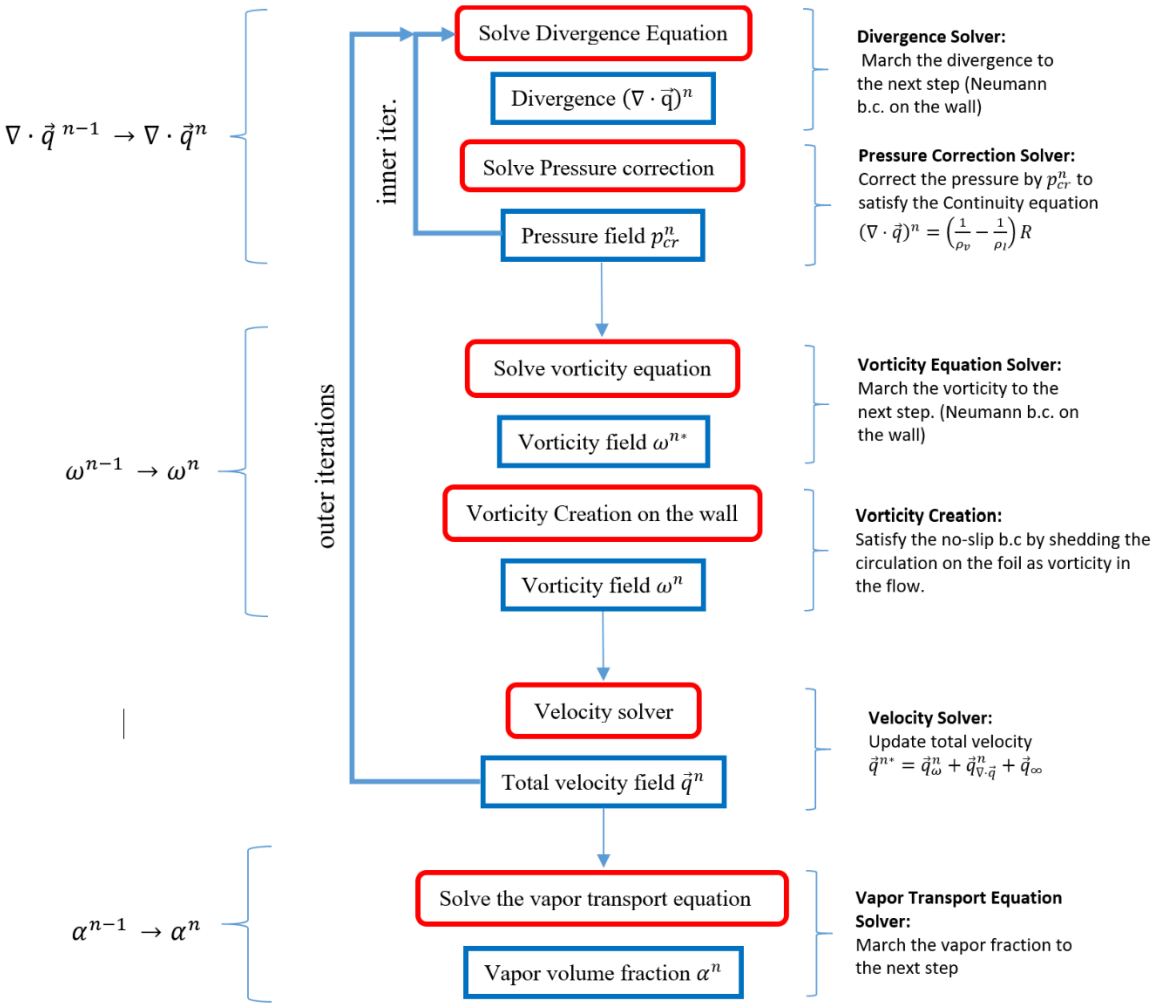

Figure 3.1: Flowchart of the general solving algorithm within a time step (n)

There are three main parts to this algorithm:

- sources update, $\nabla \cdot \vec{q}^{\,n-1} \rightarrow \nabla \cdot \vec{q}^{\,n}$
- vorticity update, $\omega^{n-1} \rightarrow \omega^{n}$
- vapor volume fraction update, $\alpha^{n-1} \rightarrow \alpha^{n}$

The first step is updating the sources, which requires solving DIVE. However, the divergence of velocity should also satisfy the continuity equation, which as it will be

explained later has the evaporation rate, R(p), as a forcing term on the right-hand side and depends on the pressure distribution. The DIVE and the continuity equation are solved using the SIMPLEC algorithm, that allows for the iterative solution of pressure coupled equations by applying a series of pressure corrections, p_{cor}^{n}, to the pressure of the previous time step, p^{n-1}. With the updated value of $\nabla \cdot \vec{q}^{\,n}$, the velocity field changes, which in turn changes the value of the explicit terms in the right-hand side of DIVE[1]. Therefore, it is important to repeat the process until the explicit terms converge.

The vorticity is updated by solving the VISVE, with Neumann boundary conditions on the foil (no flux of vorticity from the wall). Given that the actual boundary condition of vorticity is not known at the foil, the resulting velocity field does not satisfy the boundary condition. A correction on top of ω^{n*} is necessary to represent the vorticity creation on the wall and enforce the boundary conditions (both no-slip and no-penetrating) [10].

The outer iterations are necessary for the velocity field to converge. The vapor fraction needed for the calculation of the mixture properties is updated only once each time-step [13], since the mixture properties do not vary significantly between timesteps.

3.2 VELOCITY SOLVER

The velocity field, $\vec{q}$, can be decomposed to a divergence free component $\vec{q}_{\omega}$, a rotational free component $\vec{q}_{\vec{\nabla}\cdot\vec{q}}$ and a uniform field $\vec{q}_{\infty}$.

$$\vec{q} = \vec{q}_{\omega} + \vec{q}_{\vec{\nabla}\cdot\vec{q}} + \vec{q}_{\infty} \tag{3.1}$$

where $\vec{\nabla} \cdot \vec{q}_{\omega} = 0$ and $\vec{\nabla} \times \vec{q}_{\vec{\nabla}\cdot\vec{q}} = \vec{0}$. It can be shown that there is a stream function $\vec{\psi}$ and a velocity potential ξ, such that:

$$\vec{\nabla}\xi := \vec{q}_{\nabla\cdot\vec{q}} \qquad and \qquad \vec{\nabla} \times \vec{\psi} := \vec{q}_{\omega} \tag{3.2}$$

[1] The initial approximation p^{n-1} does not change since it is the pressure of the previous time step.

According to the definition of vorticity $\vec{\omega} := \nabla \times \vec{q}$, we have:

$$\nabla \times \left(\nabla \times \vec{\psi}\right) = \vec{\omega} \tag{3.3}$$

Using the vector identity $\vec{\nabla} \times \left(\vec{\nabla} \times \vec{\psi}\right) \equiv \vec{\nabla}\left(\vec{\nabla} \cdot \vec{\psi}\right) - \nabla^2\vec{\psi}$ and assuming two-dimensional flows, equation (3.3) becomes the scalar equation:

$$\nabla^2\psi = -\omega \tag{3.4}$$

where we assumed that $\vec{\nabla} \cdot \vec{\psi} = 0$, since the definition of vorticity induced velocity (3.2) uses only the rotational part of the stream function, and therefore it does not affect the velocity field. A similar equation for the velocity potential can be obtained by taking the divergence of velocity:

$$\nabla^2\xi = \vec{\nabla} \cdot \vec{q} \tag{3.5}$$

Both the vorticity, ω, and the divergence of velocity, $\vec{\nabla} \cdot \vec{q}$, are treated as unknows in the VISVE and DIVE models. The Poisson's equations can be solved via the Green's identity for the Laplacian in *free space* [36]

$$\psi\left(\vec{x}_f\right) = \int_{\Omega} \omega(x) \;\; G\left(\vec{x}, \vec{x}_f\right) d\Omega + \psi_\infty \tag{3.6}$$

$$\xi\left(\vec{x}_f\right) = \int_{\Omega} \left(\nabla \cdot \vec{q}(x)\right) \; G\left(\vec{x}, \vec{x}_f\right) d\Omega + \xi_\infty \tag{3.7}$$

where, $\vec{x}_f = (x_f, y_f)$ is the field point and $\vec{x} = (x, y)$ is the dummy variable running over the computational domain Ω. $G\left(x, x_f\right) = (\ln\ |\vec{x} - \vec{x}_f|)/2\pi$ is the two-dimensional Green's function. $\psi_\infty$and ξ_∞, are the stream function and velocity potential corresponding to the background flow, $\vec{q}_\infty := \vec{\nabla} \times \vec{\psi}_\infty + \vec{\nabla}\xi_\infty$.

By taking the curl of equation (3.6) and divergence of equation (3.7), with respect to the field point $\vec{x}_f$ we get an expression for the total velocity field as shown in equation (3.8):

$$\vec{q} = \frac{1}{2\pi}\int_{\Omega} \omega \times \frac{\vec{r}}{r^2} + \left(\vec{\nabla} \cdot \vec{q}\right) \frac{\vec{r}}{r^2}\, d\Omega + \vec{q}_\infty \tag{3.8}$$

where, $\vec{r} = \vec{x} - \vec{x}_f = (r_x, r_y)$**.** Note that since equation (3.8) does not include the effects of the boundary, meaning that the calculated velocity on the foil will not satisfy the boundary conditions there.

Based on relation (3.8), we can define the influence coefficients for the computational cell a $\delta\Omega$ with constant vorticity ($\omega = 1$) and sources ($\nabla \cdot \vec{q} = 1$). Specifically, in the case of a cartesian coordinate system, the influence coefficients for the x and y direction are:

$$I_{\nabla\cdot\vec{q},x} = I_{\omega,y} = \frac{1}{2\pi}\int_{\delta\Omega} \frac{r_x}{r^2}\, d\Omega \tag{3.9}$$

$$I_{\nabla\cdot\vec{q},y} = -I_{\omega,x} = \frac{1}{2\pi}\int_{\delta\Omega} \frac{r_y}{\mathrm{r}^2}\, \mathrm{d}\Omega \tag{3.10}$$

where $I_{\nabla\cdot\vec{\mathrm{q}}}$ and I_{ω} are the influence coefficient for the divergence and vorticity induced velocity fields respectively. Those integrals only need to be evaluated once at the pre-processing stage to calculate the influence coefficients, which can be re-used at each time step.

Discretizing the domain Ω and assuming constant vorticity and sources over each computational cell $\delta\Omega_i$, the total velocity can be written as:

$$q_j = \sum_i \left(I_{\omega,j}\,\omega + I_{\nabla\cdot\vec{q},j}\,\vec{\nabla}\cdot\vec{q}\right)_i + \vec{q}_{\infty,j} \tag{3.11}$$

where the j index corresponds to either the x or y direction. Once the vorticity and divergence of velocity are found, the velocity induced by the vortex and source singularity can be uniquely obtained from relation (3.11).

Alternatively, we could solve equations (3.4) and (3.5) using a Poisson solver (see section 3.10) to obtain the stream function, ψ, and velocity potential, ξ, and then taking their gradients to calculate the velocity. In that case, we could specify either a Neumann or

a Dirichlet boundary condition for ψ and ξ at the wall, corresponding to the no-through and no-slip boundary conditions respectively.

3.3 PRESSURE CALCULATION

Though pressure is not a direct solution out of vorticity equation, we need pressure to evaluate the cavitation phenomenon, which is essentially driven by the pressure change. Unlike RANS, where the computational domain extends to the point where the gauge pressure is zero at the inflow, VISVE has a smaller domain and therefore the pressure at the inflow is not zero. On the other hand, the pressure correction, p_{cr}, has a zero value[2] at the inflow, requiring a first approximation of pressure, p_0, at each time step. Therefore, an additional pressure calculation subroutine needs to be developed.

Starting from the momentum equation in the direction normal to the hydrofoil surface and assuming steady and incompressible flow, we can solve for the pressure. In this case we ignore the gravitational terms for simplicity. A detailed derivation of the formula is given in Appendix A. The result is shown in the following equation:

$$\frac{\partial p_0}{\partial n} = -\rho \frac{\partial}{\partial n}\left(\frac{1}{2}q^2\right) + \rho(\vec{n} \times \vec{q}) \cdot \vec{\omega} - \mu\left(\vec{V} \times \vec{\omega}\right) \cdot \vec{n} \qquad (3.12)$$

where t is time, p_0 is the first approximation of pressure, ρ is density, μ is the dynamic viscosity, $\vec{q}$ is the total velocity, $\vec{\omega}$ is vorticity, μ is dynamic viscosity, and $\vec{n}$ is direction to the hydrofoil surface. This first approximation only accounts for the pressure component due to the convection and diffusion terms in the momentum equation. The residual viscous pressure terms are included in the pressure correction p_{cr}.

Since in VISVE the grid is generated normal to the hydrofoil, a line integral can be conducted along the direction normal to the hydrofoil from the outer boundary $\left(x_f\right)$ to any point (x) within the domain to calculate the pressure at that point. The integral paths are

[2] Of course, the inflow should be far enough from the foil so that the assumption, $p_{cr} = 0$, is valid.

shown as red arrowed lines in Figure 3.2. Therefore, as long as the pressure boundary condition is given, the pressure within the whole domain can be obtained.

$$p_x = p_{boundary}(x_f) + \int_{boundary\ x_f}^{X} \frac{\partial p}{\partial n} \cdot dn \tag{3.13}$$

where the inlet pressure at the boundary is calculated using the Bernoulli equation for steady, inviscid flows.

$$p_{boundary}(x_f) = p_\infty + \frac{1}{2}\rho_l\left(q_\infty^2 - q^2(x_f)\right) \tag{3.14}$$

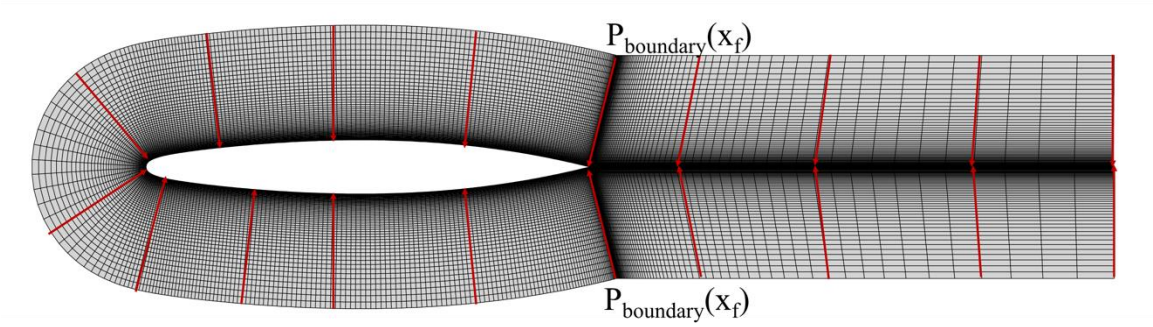

Figure 3.2: Pressure evaluation scheme illustration

Given that the flow will eventually reach a steady state, the unsteady term both in (3.13) and (3.14) can be neglected for simplicity. Until a steady state is reached, however, the first approximation of pressure field might exhibit discontinuities at the trailing edge and the wake since the pressure at those points is calculated starting from different points of the inflow boundary (see Figure 3.2).

Note that by integrating along one direction, the continuity of pressure is guaranteed only in the direction normal to the foil. In other words, since we do not solve a system for the pressure, adjacent strips might exhibit discontinuity.

3.4 CONTINUITY EQUATION ENFORCEMENT

In this thesis, the cavitating flows are modeled as one homogeneous mixture of a liquid and a vapor phase. Each phase is described by a volume fraction parameter, a_i, and all the phases must fill up the available volume, leading to the following constraint [13]:

$$a_v + a_l = 1 \tag{3.15}$$

Since there are only two phases, we can define $a \coloneqq a_v$ as the vapor volume fraction, so the liquid volume fraction becomes $a_l = 1 - a$. The density (ρ_m) and dynamic viscosity (μ_m) of the mixture, are defined in equation (3.16) based on the homogeneous flow assumptions:

$$\rho_m = \alpha\rho_v + (1-\alpha)\rho_l \;\; ; \quad \mu_m = \alpha\mu_v + (1-\alpha)\mu_l \tag{3.16}$$

where ρ_v, ρ_l is the density of the vapor phase and the fluid phase; $\mu_v,\ \mu_l$ is the dynamic viscosity of the vapor phase and the fluid phase. Both phases are assumed to be incompressible ($\rho_l,\ \rho_v = constant$) and share the same velocity field. Equation (3.17) represents the conservation of mass for each phase, i, [13]:

$$\frac{\partial a_i\,\rho_i}{\partial t} + \vec{\nabla}\cdot(a_i\,\rho_i\vec{q}) = R_i \tag{3.17}$$

where ρ_i, a_i and R_i , represent respectively the density, the volume fraction and the mass generation of phase i. We have also assumed that the mass sources, R_i, arise from interphase mass transfer and therefore satisfy the constrain [13]:

$$R_v + R_l = 0 \tag{3.18}$$

Again, we can simplify the notation by setting $R \coloneqq R_v$ and $R_l = -R$. There are a few different models describing the phase change rate ($R = R_e$ in case of evaporation; $R = R_c$ in case of condensation) two of which will be discussed in section 3.5. Notice that this condition implies the mass conservation of the mixture:

$$\frac{\partial \rho_m}{\partial t} + \vec{\nabla} \cdot (\rho_m \vec{q}) = 0 \tag{3.19}$$

The two equations for the conservation of mass, (3.17), are equivalent to the following system:

$$\frac{\partial \alpha}{\partial t} + \vec{\nabla} \cdot (\alpha\, \vec{q}) = \frac{R}{\rho_v} \tag{3.20}$$

$$\vec{\nabla} \cdot \vec{q} = R\left(\frac{1}{\rho_v} - \frac{1}{\rho_l}\right) \tag{3.21}$$

The first equation is the mass conservation for the vapor and by subtracting with the second one we get the mass conservation for the liquid. Equation (3.20) is the vapor transport equation, while equation (3.21) models the "compressibility" of the mixture due to the generation and collapse of cavity bubbles and will be called as continuity equation in the rest of the literature. The boundary conditions for equation (3.20) are:

$$\textit{Vapor transport equation:} \begin{cases} wall & : \quad - \\ inflow: & Dirichlet\ b.c.\ (a = 0) \\ outflow: & Neumann\ b.c.\left(\frac{\partial a}{\partial n} = 0\right) \end{cases} \tag{3.22}$$

Notice that there is no need for a wall boundary condition for the vapor transport since it a first order differential equation in space. Specifically, the vapor flux, $a \cdot \vec{q}$, on the wall is zero due to the no through boundary condition.

Given a characteristic length L, and velocity U, equation (3.20) can be brought to the following non-dimensional form:

$$\frac{\partial \alpha}{\partial t^*} + \vec{\nabla}^* \cdot (\alpha\, \vec{q}^*) = R^* \tag{3.23}$$

where $t^* \coloneqq t\frac{U}{L}$, $\vec{q}^* = \frac{\vec{q}}{U}$, $\vec{\nabla}^* \cdot \coloneqq L\,\nabla \cdot$ and $R^* \coloneqq \frac{R\,U}{\rho_v\, L}$. Therefore, the empirical coefficients involved in R should change depending on the characteristic time scale $T \coloneqq L/U$ of the problem. These non-dimensional parameters are the same for the continuity equation (3.21).

3.5 PHASE CHANGE MODELS

The phase change rate (R) has been involved in both the continuity equation and the vapor transport equation. There are several broad categories of models to evaluate these source terms as discussed in Section 2.2.2. The predominant approaches are based on the simplified form Rayleigh-Plesset equation [12, 13] to formulate the simple rational expression. The general form of Rayleigh-Plesset equation has been presented in equation (2.4), which is too complicated to be applied to any multiphase cavitation model. Here, several assumptions need to be made to simplify the equation:

- There are plenty of nuclei for the inception of cavitation, so the term related to initial stage can be ignored.
- The surface tension force can be neglected.
- Only first-order terms are considered significant.

Then the Rayleigh-Plesset equation can be reduced to:

$$\frac{d\Re_B}{dt} = \sqrt{\frac{2}{3}\frac{(P_v - P_\infty)}{\rho_l}} \tag{3.24}$$

The above equation provides a feasible and physical approach to introduce the bubble dynamics into the cavitation models. In our work, we applied the model proposed by Schnerr and Sauer [12] and the model by Zwart- Gerber- Belamri [13]. Results from the model proposed by Zwart- Gerber- Belamri [13] will be presented in this thesis.

3.5.1 Schnerr and Sauer's Model

Starting from the mass conservation for the mixture (3.19) in its convective form and substituting equation (3.16), we get:

$$\vec{\nabla} \cdot \vec{q} = -\frac{1}{\rho_m}\left(\frac{d\rho_m}{dt}\right) = \frac{\rho_l - \rho_v}{\rho_m}\left(\frac{da}{dt}\right) \tag{3.25}$$

Comparing equation (3.25) to the continuity equation (3.21) we get an expression for the net phase change rate [12]:

$$R = \frac{\rho_v \rho_l}{\rho_m}\left(\frac{d\alpha}{dt}\right) \tag{3.26}$$

and then the vapor volume fraction is defined as the ratio of the volume of vapor over the cell volume and then reformulated:

$$\alpha := \frac{V_{vapor}}{V_{cell}} = \frac{N_{bubbles} \cdot \frac{4}{3}\pi \Re_B{}^3}{V_{vapor} + V_{liquid}} = \frac{n_0 V_{liquid} \cdot \frac{4}{3}\pi \Re_B{}^3}{n_0 V_{liquid} \cdot \frac{4}{3}\pi \Re_B{}^3 + V_{liquid}} \tag{3.27}$$

where V_{vapor}, V_{liquid}, V_{cell} represent the volume of vapor, liquid, and cell respectively; $\Re_B$ is the radius of the vapor bubble; $n_0 := \mathrm{N_{bubbles}}/V_{liquid}$ is the bubble concentration per unit volume of pure liquid and is set to be $10^{13}(m^{-3})$ [12]. Taking the time derivative of relation (3.27) we get:

$$\frac{da}{dt} = \left[1 - \frac{V_{vapor}}{V_{cell}}\right]\frac{1}{V_{cell}}\frac{d}{dt}\left(V_{vapor}\right) = (1-a)a\frac{3}{\Re_B}\frac{d\Re_B}{dt} \tag{3.28}$$

Combining equations (3.26) and (3.28), the evaporation and condensation phase change rate is then modeled from Rayleigh-Plesset equation as follows:

$$R_e = \frac{\rho_l \rho_v}{\rho_m}\alpha(1-\alpha)\frac{3}{\Re_B}\sqrt{\frac{2}{3}\frac{(p_V - p)}{\rho_l}}, \qquad when\ p < p_V \tag{3.29}$$

$$R_C = \frac{\rho_l \rho_v}{\rho_m}\alpha(1-\alpha)\frac{3}{\Re_B}\sqrt{\frac{2}{3}\frac{(p - p_V)}{\rho_l}}, \qquad when\ p > p_V \tag{3.30}$$

Notice that in the case of $a = 1$ and $a = 0$, there is neither evaporation nor condensation, therefore this model implies the presence of dissolved gases or dispersed vapor in the fluid. Moreover, it is possible to determine the bubble radius, $\Re_B$, based on the bubble density, n_0:

$$\Re_B = \left(\frac{\alpha}{1-\alpha}\frac{3}{4\pi}\frac{1}{n_0}\right)^{\frac{1}{3}} \tag{3.31}$$

For different length, L, and velocity, U, scales, the bubble radius and therefore the bubble density should be adjusted in order to obtain a similar cavity, assuming of course similar cavitation and Reynolds numbers.

3.5.2 Zwart- Gerber- Belamri's Model

This model assumes constant bubble radius implying a fixed cell volume ($V_{cell} = constant$) and proposes that the total interphase mass transfer rate, R, can be calculated using the bubble density number, $n := \mathrm{N}_{\mathrm{bubbles}} / V_{cell}$ and the mass change rate of a single bubble [13].

$$R = \frac{d}{dt}\left(\rho_v \frac{V_{vapor}}{V_{cell}}\right) = \rho_v \cdot \frac{d}{dt}\left(n\frac{4}{3}\pi\Re_B^3\right) = \frac{3\alpha\rho_v}{\Re_B}\frac{d\Re_B}{dt} \tag{3.32}$$

where the vapor volume fraction, α, can be related to the bubble number density, n and bubble radius, $\Re_B$, as

$$\alpha = n\left(\frac{4}{3}\pi\Re_B^3\right) \tag{3.33}$$

Substituting the Rayleigh-Plesset equation into (3.32), we can obtain the expression of the mass transfer rate as:

$$R = \frac{3\alpha\rho_v}{\Re_B}\sqrt{\frac{2}{3}\frac{p_V - p}{\rho_v}} \tag{3.34}$$

The Rayleigh-Plesset equation and therefore equation (3.34) is derived for evaporation process. To generalize it to both evaporation and condensation process, several empirical coefficients are introduced, which yield:

$$R_e = F_{evap}\frac{3\alpha_{nuc}(1-\alpha)\rho_v}{\Re_B}\sqrt{\frac{2}{3}\frac{(p_V - p)}{\rho_l}} \tag{3.35}$$

$$R_C = F_{cond}\frac{3\alpha\rho_v}{\Re_B}\sqrt{\frac{2}{3}\frac{(p - p_V)}{\rho_l}} \tag{3.36}$$

In the above equations, α_{nuc} is the nucleation site volume fraction, F_{evap} and F_{cond} are two empirical calibration coefficients for the evaporation and condensation process, respectively. The default value for those parameters are $\alpha_{nuc} = 5.0 \times 10^{-4}$, $\Re_B = 1.0 \times 10^{-6} m$, $F_{evap} = 50$, $F_{cond} = 0.01$.

For different length, L, and velocity, U, scales, the bubble radius should be adjusted in order to obtain a similar cavity, assuming of course similar cavitation and Reynolds numbers.

3.6 DIVERGENCE EQUATION

In order to present the 2-D divergence equation, we have to start from the Navier Stokes equations:

$$\rho \frac{\partial \vec{q}}{\partial t} + \rho(\vec{q} \cdot \vec{\nabla})\vec{q} = -\nabla p + \nabla \cdot \bar{\bar{T}} \tag{3.37}$$

The pressure is split into two components:

$$p = p_0 + p_{cor} \tag{3.38}$$

where p_0 is the first approximation of the pressure given by relation (3.12), that takes only the wetted-flow terms into consideration and p_{cr} is the pressure correction term resulting from the pressure correction method, which will be discussed in the next section. By definition

$$-\vec{\nabla} \cdot \left(\frac{\vec{\nabla} p_0}{\rho}\right) := \vec{\nabla} \cdot \left((\vec{q} \cdot \vec{\nabla})\vec{q} + \nu_m \vec{\nabla} \times \vec{\omega}\right) \tag{3.39}$$

Taking the divergence of relation (3.37) we obtain the divergence equation:

$$\frac{\partial(\vec{\nabla} \cdot \vec{q})}{\partial t} = \vec{\nabla} \cdot \left[\nu_m \vec{\nabla}(\nabla \cdot \vec{q})\right] + P_{cor,\vec{\nabla}\cdot\vec{q}} + Q_{\vec{\nabla}\cdot\vec{q}} \tag{3.40}$$

Where

$$P_{cor,\vec{\nabla}\cdot\vec{q}} := -\vec{\nabla}\cdot\left(\frac{\vec{\nabla}p_{cor}}{\rho}\right) \tag{3.41}$$

$$\begin{aligned} Q_{\nabla\cdot\vec{q}} &:= \vec{\nabla}\cdot\left(\frac{1}{\rho}\vec{\nabla}\cdot\bar{\bar{T}}\right) - \vec{\nabla}\cdot\left(\nu_m\vec{\nabla}(\vec{\nabla}\cdot\vec{q})\right) = \\ &= \left(\frac{\vec{\nabla}\mu}{\rho}\right)\cdot\vec{\nabla}(\vec{\nabla}\cdot\vec{q}) - \left(\vec{\nabla}\nu_m + \frac{\vec{\nabla}\mu}{\rho}\right)\times\vec{\nabla}\omega \\ &\quad + \left[\left(\frac{\mu_y}{\rho}\right)_x + \left(\frac{\mu_x}{\rho}\right)_y\right](v_x + u_y) + \left[\left(\frac{\mu_x}{\rho}\right)_x - \left(\frac{\mu_y}{\rho}\right)_y\right](u_x - v_y) \end{aligned} \tag{3.42}$$

are the pressure sources and residual viscous terms respecitively, for the divergence equation in a cartesian coordinate system; $\nu_m := \frac{\mu}{\rho}$ is the molecular kinematic viscosity of the mixture[3]; u is the velocity component in the x-direction and v is the velocity component in the y-direction. The subscripts of x and y indicate partial derivative in the x and y direction, respectively. Notice that $Q_{\vec{\nabla}\cdot\vec{q}} = 0$, in the case of constant density and dynamic viscosity. The analytic derivation of relation (3.42) is shown in appendix B.

In equation (3.40) the term $\vec{\nabla}\cdot\vec{q}$ is treated as an unknow which should also satisfy the continuity equation (3.21). The two equations are solved iteratively, using the SIMPLEC algorithm [37], until convergence. The first approximation of pressure, p_0, is then updated based on the updated velocity field (outer iterations) and the process starts over. An alternative formulation for the divergence equation is presented in appendix C.

The boundary conditions for equations (3.40) are:

$$\textit{Divergence equation:} \begin{cases} wall: Neumann\ b.c.\left(\frac{\partial\nabla\cdot\vec{q}}{\partial n} = 0\right) \\ inflow: Dirichlet\ b.c.\ (\nabla\cdot\vec{q} = 0) \\ outflow: Neumann\ b.c.\left(\frac{\partial\nabla\cdot\vec{q}}{\partial n} = 0\right) \end{cases} \tag{3.43}$$

[3] The subscript m for ν_m was used to differentiate the viscosity from the y-component of velocity v

The computational domain over which the DIVE is solved can be much smaller than the VISVE domain, as long as it includes the cavity. For simplicity we solve DIVE over the whole domain with the same boundary conditions as VISVE. The boundary condition at the wall on the is not known, so we assume it to be Neumann boundary condition. We only require that the total velocity, $\vec{q}$, is zero at the wall, which we accomplish by the vorticity creation algorithm.

3.7 PRESSURE CORRECTION EQUATION SOLVER

3.7.1 Mathematical Formulation

The divergence equation (3.40) can be written in the following matrix form where the unknowns are kept on the left-hand side and the forcing terms on the right-hand side:

$$A_D\left(\vec{\nabla}\cdot\vec{q}\right) + A_{OD}\left(\vec{\nabla}\cdot\vec{q}\right) = -\vec{\nabla}\cdot\left(\frac{\vec{\nabla}p_{cor}}{\rho}\right) + Q_{\vec{\nabla}\cdot\vec{q}} \tag{3.44}$$

where $A = A_D + A_{OD}$ is the coefficient matrix of the divergence equation, with A_D being the matrix with the diagonal elements of A and A_{OD} the matrix with the off-diagonal elements. Given that the divergence equation is solved iteratively, after m iterations we have the values $\left(\vec{\nabla}\cdot\vec{q}\right)^m, p_{cor}^m$. If the current timestep is n then, for m=0, $\left(\vec{\nabla}\cdot\vec{q}\right)^m$=$\left(\vec{\nabla}\cdot\vec{q}\right)^n$ and for $m\to\infty$, $\left(\vec{\nabla}\cdot\vec{q}\right)^m \to \left(\vec{\nabla}\cdot\vec{q}\right)^{n+1}$. Note that during those m iterations, the values of p_0 and $Q_{\vec{\nabla}\cdot\vec{q}}$ have not changed.

Given the pressure correction, p_{cor}^{m-1} at iteration $m-1$, $\left(\vec{\nabla}\cdot q\right)^{m-1}$ can be calculated from the divergence equation as:

$$A_D\left(\vec{\nabla}\cdot\vec{q}\right)^{m-1} + A_{OD}\left(\vec{\nabla}\cdot\vec{q}\right)^{m-1} = -\vec{\nabla}\cdot\left(\frac{\vec{\nabla}p_{cor}^{m-1}}{\rho}\right) + Q_{\vec{\nabla}\cdot\vec{q}} \tag{3.45}$$

The corresponding equation for iteration m, is:

$$A_D\left(\vec{\nabla}\cdot\vec{q}\right)^m + A_{OD}\left(\vec{\nabla}\cdot\vec{q}\right)^m = -\vec{\nabla}\cdot\left(\frac{\vec{\nabla}p_{cor}^m}{\rho}\right) + Q_{\vec{\nabla}\cdot\vec{q}} \tag{3.46}$$

where the divergence satisfies the continuity equation, $\left(\vec{\nabla}\cdot\vec{q}\right)^m = \left(\frac{1}{\rho_v}-\frac{1}{\rho_l}\right)R(p^m)$ and the value of pressure, p^m and therefore the value of p_{cor}^m is to be determined. In the case of the SIMPLE (Semi-Implicit Method for Pressure Linked Equations) algorithm, the off-diagonal terms in equation (3.52) are approximated using the values of the previous iteration.

$$A_{OD}\left(\vec{\nabla}\cdot\vec{q}\right)^m \approx A_{OD}\left(\vec{\nabla}\cdot\vec{q}\right)^{m-1} \tag{3.47}$$

while in the case of SIMPLEC (Semi-Implicit Method for Pressure Linked Equations Corrected) algorithm, the following linear approximation is used, for the coefficients of the i-th equation:

$$\left(\vec{\nabla}\cdot\vec{q}\right)_i^m \sum_k A_{OD,k} \approx \sum_k A_{OD,k}\left(\vec{\nabla}\cdot\vec{q}\right)_k^m \tag{3.48}$$

Subtracting equations (3.45) and (3.46) we obtain:

$$\tilde{A}_D\left(\vec{\nabla}\cdot\vec{q}\right)^m + \vec{\nabla}\cdot\left(\frac{\vec{\nabla}p^m}{\rho}\right) = \tilde{A}_D\left(\vec{\nabla}\cdot\vec{q}\right)^{m-1} + \vec{\nabla}\cdot\left(\frac{\vec{\nabla}p^{m-1}}{\rho}\right) \tag{3.49}$$

where $\tilde{A}_D$ is a diagonal matrix with the i-th element being $\tilde{A}_{D,i} := A_{D,i}$ for the SIMPLE method and $\tilde{A}_{D,i} := A_{D,i} + \sum_k A_{OD,k}$ for the SIMPLEC method. Notice that since p_0 does not change between iterations $m-1$ and m, equation (3.49) uses the total pressure, p, instead of the pressure correction.

Both cavitation models described in section 3.5 use the Rayleigh-Plesset equation and as a result the phase change rate is proportional to the square root of pressure $\left(R\sim\sqrt{|p-p_v|}\right)$. Therefore, the continuity equation at the m-th iteration can be written as:

$$\left(\vec{\nabla}\cdot\vec{q}\right)^m = \left(\frac{1}{\rho_v}-\frac{1}{\rho_l}\right)R = C\sqrt{|p^m-p_v|} \tag{3.50}$$

where $C \coloneqq \left(\frac{1}{\rho_v} - \frac{1}{\rho_l}\right)\frac{R}{\sqrt{|p-p_v|}}$ is the proportionality constant which depends on the vapor volume fraction and the cavitation model being used. Note, that the C coefficient has a discontinuity at $p = p_v$, due to the fact the cavitation models have different coefficients for evaporation and condensation.

Substituting equation (3.50) into equation (3.49) we obtain the pressure correction equation.

$$\vec{\nabla} \cdot \left(\frac{\vec{\nabla} p^m}{\rho}\right) + \tilde{A}_D C^m \sqrt{|p^m - p_v|} = \tilde{A}_D \left(\vec{\nabla} \cdot \vec{q}\right)^{m-1} + \vec{\nabla} \cdot \left(\frac{\vec{\nabla} p^{m-1}}{\rho}\right) \tag{3.51}$$

When equation (3.51) converges, we get back the continuity equation (3.21). Notice that at points where $\vec{\nabla} \cdot \vec{q} \neq 0 \Rightarrow p \neq p_v$. Therefore, the pressure underneath the cavity is not necessarily equal to vapor pressure. However, the greater the value of the phase change rate coefficient, C, is, the closer the value of p is to p_v. When calculating the pressure coefficient at chapter 4, we force the condition $p \geq p_v$, which in turn results in a constant pressure coefficient underneath the cavity.

3.7.2 Linearization of Pressure Correction Equation

The pressure correction equation as described above is a non-linear equation due to the square root. Linearizing the equation using Newton's approximation for the p variable, $\sqrt{x} \approx \sqrt{x_0} + \frac{dx}{2\sqrt{x_0}}$, inhibits the convergence due to the overshooting of the solution when $p \to p_v$. We can eliminate the square root by solving for q (not the velocity $\vec{q}$) which is defined as:

$$q \coloneqq \sqrt{|p - p_v|} \quad \Rightarrow \quad p = p_v - sign(C)\, q^2 \tag{3.52}$$

with $sign(C) = sign\left(\vec{\nabla} \cdot \vec{q}\right) = -sign(p - p_v)$. The pressure term in the pressure correction equation (3.51), can therefore be expressed as:

$$\vec{\nabla}\cdot\left(\rho^{-1}\vec{\nabla}p\right) = -sign(C)\vec{\nabla}\cdot\left(2q\,\rho^{-1}\vec{\nabla}\mathrm{q}\right)\ ,\quad (\,q\neq 0\,) \tag{3.53}$$

The above relation is true for all the values of q except q=0. Note that for any given p, the value of $sign(C)$ is constant and therefore it comes out of the derivatives. Relation (3.53) implies that the grid is fine enough, so that all the points in the computational molecule/stencil have the same value for $sign(C)$. Using a backwards difference method, the derivative in the x-direction can be expressed as:

$$\left(\frac{\partial p}{\partial x}\right)_i \approx -sign(C_i)2\bar{q}\frac{q_i - q_{i-1}}{x_i - x_{i-1}} - [sign(C_i) - sign(C_{i-1})]\frac{|p_{i-1} - p_v|}{x_i - x_{i-1}} \tag{3.54}$$

where the index, i, indicates the values at centroid i and $\bar{q} \coloneqq (q_i + q_{i-1})/2$. In the regions where the pressure is close to the vapor pressure ($p \approx p_v$), it is possible to have $sign(C_i) = -sign(C_{i-1})$.In that case there is $x_0 \in (x_{i-1}, x_i)$ such that $p(x_0) = p_v$ and for $x_{i-1} < x_0$:

$$\left|\frac{p_{i-1} - p_v}{x_i - x_{i-1}}\right| \leq \beta\left|\frac{p_v - p_{i-1}}{x_0 - x_{i-1}}\right| \leq \gamma\left|\left(\frac{\partial p}{\partial x}\right)_{x_0^-}\right| \tag{3.55}$$

where β and γ are constants. Therefore, the error due to the discontinuity of pressure is bounded by the local pressure gradient at the edge of the cavity. The pressure inside the cavity is constant and therefore $\frac{\partial p}{\partial x} = 0$. Assuming that the pressure distribution has a continuous pressure gradient, then for a fine enough discretization the points outside of the cavity will have a very small pressure gradient $\left(\frac{\partial p}{\partial x} \to 0\right)$ which minimizes the error in equation (3.54). Using relation (3.52), the pressure correction equation (3.51) becomes:

$$-sign(C^{m-1})\,\vec{\nabla}\cdot\left(\frac{2q^{m-1}\vec{\nabla}\delta q^m}{\rho}\right) + \tilde{A}_D C^{m-1}\delta q^m = \tilde{A}_D\left[\left(\vec{\nabla}\cdot\vec{q}\right)^{m-1} - C^{m-1}q^{m-1}\right] \tag{3.56}$$

where $\delta q^m \coloneqq q^m - q^{m-1} = \sqrt{|p^m - p_v|} - \sqrt{|p^{m-1} - p_v|}$ and the non-linear terms are kept at the previous iteration, including the cavitation coefficient, $C^m = C^{m-1}$.

The boundary value of q on the wall depends on the boundary value of the pressure there, which is unknown, so we assume that $\partial\delta q/\partial n = 0$ on the wall. Far away from the cavity the pressure correction should have a very small value, so we can impose either a Neumann or Dirichlet b.c.

$$Pressure\ Correction\ eqn:\ \begin{cases} wall: \ \ Neumann\ b.c.\left(\frac{\partial \delta q}{\partial n}=0\right) \\ inflow: \ \ Dirichlet\ b.c.\ \ (\delta q=0) \\ outflow: Neumann\ b.c.\left(\frac{\partial \delta q}{\partial n}=0\right) \end{cases} \tag{3.57}$$

Equation (3.56) is an elliptic type equation, which can be solved using the ADI method. Specifically, instead of solving (3.56) directly, we try to find the steady state solution to the following unsteady problem:

$$\frac{\partial \delta q^m}{\partial t}+\tilde{A}_D|C^{m-1}|\delta q^m-\vec{\nabla}\cdot\left(\frac{2q^{m-1}\vec{\nabla}\delta q^m}{\rho}\right)=sign(C^{m-1})\,\tilde{A}_D\left[\left(\vec{\nabla}\cdot\vec{q}\right)^{m-1}-C^{m-1}q^{m-1}\right] \tag{3.58}$$

3.8 2-D Viscous Vorticity Equation Solver

In order to present the 2-D viscous vorticity equation, we have to start from the Navier Stokes equations, as shown in equation (3.37).

$$\rho\frac{\partial \vec{q}}{\partial t}+\rho\left(\vec{q}\cdot\vec{\nabla}\right)\vec{q}=-\vec{\nabla}p+\vec{\nabla}\cdot\bar{\bar{T}} \tag{3.59}$$

where, ρ is the density of the fluid, p is the mean pressure, and $\bar{\bar{T}}$ is the viscous stress tensor. Using equation (A.4), equation (3.59) can be written as:

$$\frac{\partial \vec{q}}{\partial t}+\vec{\nabla}\left(\frac{1}{2}q^2\right)-\vec{q}\times\vec{\omega}=-\frac{\vec{\nabla}p}{\rho}+\frac{1}{\rho}\vec{\nabla}\cdot\bar{\bar{T}} \tag{3.60}$$

Taking the curl on both sides and using identities (D.4) and (D.5), results in the general form of the vorticity equation:

$$\frac{\partial \vec{\omega}}{\partial t}+\vec{\nabla}\cdot(\vec{q}\otimes\vec{\omega})-\left(\vec{\omega}\cdot\vec{\nabla}\right)\vec{q}=\frac{\vec{\nabla}\rho\times\vec{\nabla}p}{\rho^2}+\vec{\nabla}\times\left(\frac{1}{\rho}\vec{\nabla}\cdot\bar{\bar{T}}\right) \tag{3.61}$$

where starting from the left most term we have the unsteady term, vorticity convection[4], vortex stretching, baroclinic torque and viscous torque. In this thesis, only two-dimensional

[4] The convection term contains the tensor product of velocity and vorticity $\vec{q}\otimes\vec{\omega}=q_j\,\omega_i$ defined in (D.4).

flows are studied, where vorticity can be treated as a scalar and the vortex stretching term becomes zero. Then the 2-D viscous vorticity equation can be written as:

$$\frac{\partial \omega}{\partial t} + \vec{\nabla} \cdot (\vec{q}\ \omega) = \vec{\nabla} \cdot \left(\nu_m \vec{\nabla}\omega\right) + P_\omega + Q_\omega \tag{3.62}$$

Where

$$P_\omega := \frac{\vec{\nabla}\rho \times \vec{\nabla}p}{\rho^2} \tag{3.63}$$

$$\begin{aligned} Q_\omega &:= \vec{\nabla} \times \left(\frac{1}{\rho}\vec{\nabla} \cdot \bar{\bar{T}}\right) - \vec{\nabla} \cdot \left(\nu_m \vec{\nabla}\omega\right) = \\ &= \left(\vec{\nabla}\nu_m + \frac{\vec{\nabla}\mu}{\rho}\right) \times \vec{\nabla}\left(\vec{\nabla} \cdot \vec{q}\right) + \left(\frac{\vec{\nabla}\mu}{\rho}\right) \cdot \vec{\nabla}\omega \\ &+ \left[\left(\frac{\mu_y}{\rho}\right)_x + \left(\frac{\mu_x}{\rho}\right)_y\right](v_y - u_x) + \left[\left(\frac{\mu_x}{\rho}\right)_x - \left(\frac{\mu_y}{\rho}\right)_y\right](v_x + u_y) \end{aligned} \tag{3.64}$$

are the baroclinic torque and residual viscous terms respectively, for the vorticity equation in a cartesian coordinate system; $\nu_m := \frac{\mu}{\rho}$ is the molecular kinematic viscosity of the mixture[5]; u is the velocity component in the x-direction and v is the velocity component in the y-direction. The subscripts of x and y indicate partial derivative in the x and y direction, respectively. Notice that $Q_\omega = 0$, in the case of constant density and dynamic viscosity. The analytic derivation of relation (3.44) is shown in appendix B. An alternative method for calculating the residual viscous terms using the hydrofoil assumption cab be found in [38].

The boundary conditions for equations (3.62) are:

$$\textit{Vorticity transport equation:} \begin{cases} wall: Neumann\ b.c. \left(\frac{\partial \omega}{\partial n} = 0\right) \\ inflow: Dirichlet\ b.c.\ (\omega = 0) \\ outflow: Neumann\ b.c. \left(\frac{\partial \omega}{\partial n} = 0\right) \end{cases} \tag{3.65}$$

[5] The subscript m for ν_m was used to differentiate the viscosity from the y-component of velocity v

The inflow boundary condition assumes that there is no vorticity entering the domain and any vorticity created in the wall exits the domain through the outflow. The boundary condition at the wall on the other hand is not known, so we assume it to be Neumann (no vorticity flux from the wall). We only require that the total velocity, $\vec{q}$, is zero at the wall, which we accomplish by the vorticity creation algorithm.

3.9 WALL BOUNDARY CONDITIONS

The scheme to deal with the solid boundary conditions is shown in Figures 3.3. After solving the DIVE and the VISVE, we obtain a divergence of velocity and a vorticity field. However, velocities calculated from vorticity and sources using relation (3.8) may not satisfy the no-through and no-slip boundary conditions at the wall. A vorticity creation scheme based on the Boundary Element Method (BEM) is designed to eliminate tangential and normal velocity denoted as q_n , q_s on the wall. After assigning the newly created vorticity into cells in the first layer, the non-slip boundary condition will then be satisfied. The detailed explanation in the case of vorticity creation can be found in Tian [10].

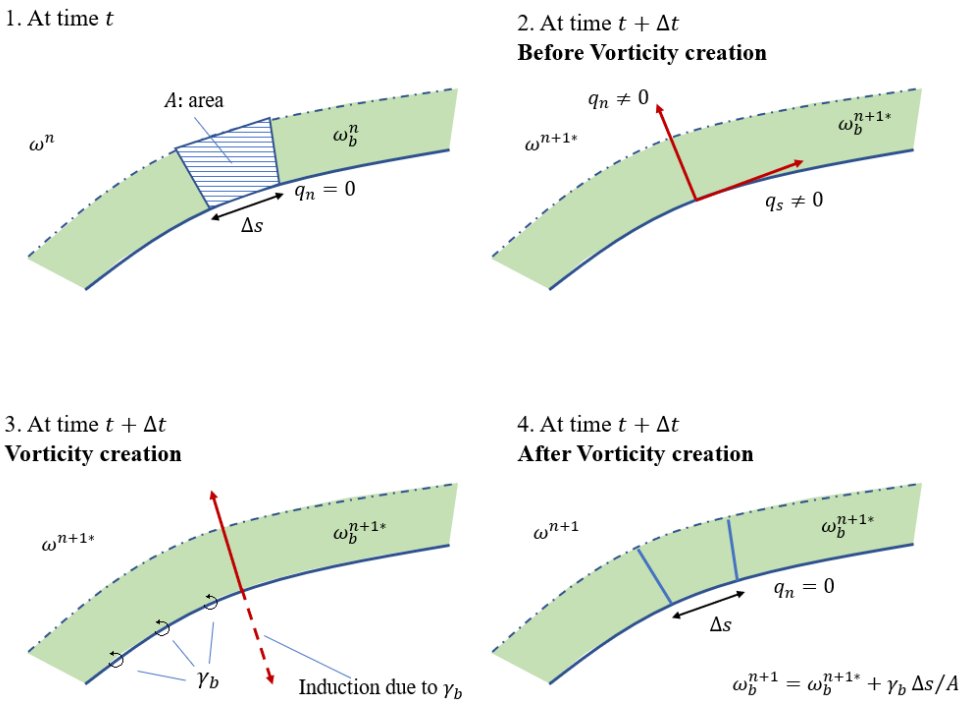

Figure 3.3: Schematic figure of the vorticity creation algorithm, from Tian [10]

For the Boundary Element Method, according the Green's 3rd identity the potential on the wall can be written as:

$$\frac{\phi}{2} = \frac{1}{2\pi}\int_S \frac{\partial \phi}{\partial n} \ln r \; ds - \frac{1}{2\pi}\int_S \phi \frac{\partial \ln r}{\partial n} \; ds \tag{3.66}$$

where S is the surface of the hydrofoil with a normal vector $\vec{n}$. The foil is discretized into N straight elements with constant source $\sigma := \frac{\partial \phi}{\partial n}$ and dipole ϕ distributions. The potential at the control point of the i-th panel is:

$$\frac{\phi_i}{2} = \sum_{j=1}^{N} \sigma_j \int_{S_j} \frac{1}{2\pi} \ln r_{ij} \; ds - \sum_{j=1}^{N} \phi_j \int_{S_j} \frac{1}{2\pi} \frac{\partial \ln r_{ij}}{\partial n_j} \; ds \tag{3.67}$$

The integrals in relation (3.72) correspond to the influence coefficient for sources, $B_{ij}$and dipoles A_{ij} from the j-panel to the i-control point and can be calculated numerically in the case of straight elements.

$$A_{ij} := \frac{1}{2\pi}\int_{S_j} \frac{\partial \ln r_{ij}}{\partial n_j}\, ds = \frac{\omega_{ij}}{2\pi} \tag{3.68}$$

$$B_{ij} := \frac{1}{2\pi}\int_{S_j} \ln r_{ij}\; ds = \frac{1}{2\pi}\left[x_0 \ln\left(\frac{r_2}{r_1}\right) + l\,(\ln r_2 - 1) + \left|y_0\omega_{ij}\right|\right] \tag{3.69}[6]$$

where the r_2 and r_1 are the distances from the left and right nodal points of panel to the control point; ω_{ij} is the angle between r_2 and r_1; x_0, y_0 is the location of the control point with respect to the local coordinate system of the panel and l is the length of the panel as show in Figure 3.4. Expressing relation (3.72) with the help of the influence coefficients we get the following system of equations:

$$\sum_{j=1}^{N} \phi_j\, A_{ij} = \sum_{j=1}^{N} \sigma_j\, B_{ij} \tag{3.70}$$

In the case of vorticity creation, the sources are defined as $\sigma = -\vec{u}\cdot\vec{n}$ and (3.75) is solved with respect to the dipoles ϕ_j. Note that solving relation (3.70) with respect to σ_j would result in a sources/sinks creation algorithm on the foil, by canceling the tangent component of velocity.

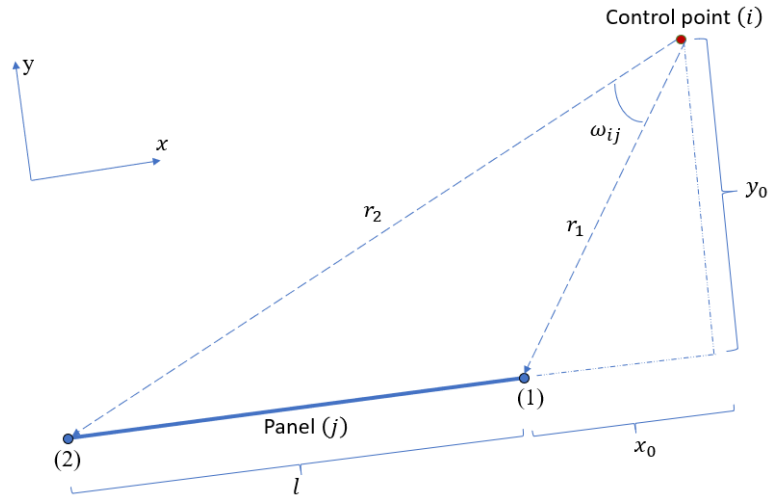

Figure 3.4: Schematic figure for the influence coefficients of panel j and control point i.

[6] $\int \ln\left(\sqrt{u^2+1}\right) du = u\cdot\ln\left(\sqrt{u^2+1}\right) - u + atan(u)\;,\quad u := (-x-x_0)/y_0$

3.10 NUMERICAL IMPLEMENTATION

3.10.1 Finite Volume Method

The equations described in the previous section can all be written in the following general form:

$$\frac{\partial \phi}{\partial t} + b\phi + \vec{\nabla} \cdot (\vec{c}\phi) - \vec{\nabla} \cdot \left(d\, \vec{\nabla}\phi\right) = R \tag{3.71}$$

For $b = 0$, we get the general form of the advection diffusion equation with the forcing term R on the right-hand side. Setting the diffusion coefficient d=0, we get the convection equation while for a zero-convection vector field, $\vec{c} = \vec{0}$, we get the diffusion equation whose steady state is the Poisson equation. Integrating over the control volume V, which in this case is a grid cell's volume, we get:

$$\int_V \left(\frac{\partial \phi}{\partial t} + b\phi\right) dV + \int_V \vec{\nabla} \cdot (\vec{c}\phi)\, dV - \int_V \vec{\nabla} \cdot \left(d\vec{\nabla}\phi\right) dV = \int_V R\, dV \tag{3.72}$$

Then, Gauss divergence theorem can be applied to equation (3.73) to transform the volume integration into surface integral:

$$\int_V \left(\frac{\partial \phi}{\partial t} + b\phi\right)\, dV + \int_S (\phi\, \vec{c} \cdot \vec{n})\, dS - \int_S \left(d\, \vec{\nabla}\phi\right) \cdot \vec{n}\ dS = \int_V R\, dV \tag{3.73}$$

where, S is the control surface, or a grid face's area.; $\vec{n}$ is the unit normal vector that pointing outside the control surface S.

If we discretize the control surface into a summation of several faces which are labeled as $1, 2, 3, \cdots, N$. Equation (3.73) can then be represented in a discretized form:

$$\left(\frac{\partial \phi}{\partial t} + bf\right) A\ + \sum_{j=1}^{N} (\phi\, \vec{c} \cdot \vec{n}\, \Delta l)_j = \sum_{j=1}^{N} \left(d \frac{\partial \phi}{\partial n} \Delta l\right)_j + R \cdot A \tag{3.74}$$

in which, subscript j denoted the values that are evaluated on the face j. It should be noted here that in two-dimensional flow, the surfaces and volume degenerate to the lengths Δl_j and area A, respectively.

In equation (3.74), $(\phi\, \vec{c} \cdot \vec{n}\, \Delta l)_j$ represent the convective terms, which can be calculated by using the modified QUICK scheme which will be discussed in the next section; $\left(d \frac{\partial \phi}{\partial n} \Delta l\right)_j$ represent the diffusive terms. In the case of the divergence and vorticity equations the forcing term R includes the gradients of various fluid properties. These gradients are calculated using the least-squares cell-based method described in Wu [5].

At this point, the space discretization has been achieved. For the time discretization the standard ADI scheme is used to solve (3.74) which is first split in two directions:

$$\frac{\partial \phi}{\partial t} = (b_1 + c_1 + d_1)\, \phi + (b_2 + c_2 + d_2)\, \phi + R \tag{3.75}$$

where $c_{1,2}$ and $d_{1,2}$ are the convective and diffusive coefficients in directions 1 and 2 respectively while $b_1 = b_2 = \frac{b}{2}$. The two ADI sweeps can be applied:

$$\begin{aligned} \phi^{n+1/2} &= \left[1 - \frac{\Delta t}{2}(b_1 + c_1 + d_1)\right]^{-1} \left\{\left[1 + \frac{\Delta t}{2}(b_2 + c_2 + d_2)\right] \phi^n + \frac{R}{2}\right\} \\ \phi^{n+1} &= \left[1 - \frac{\Delta t}{2}(b_2 + c_2 + d_2)\right]^{-1} \left\{\left[1 + \frac{\Delta t}{2}(b_1 + c_1 + d_1)\right] \phi^{n+1/2} + \frac{R}{2}\right\} \end{aligned} \tag{3.76}$$

3.10.2 QUICK scheme and flux limiter

The Quadratic Upstream Interpolation for Convective Kinematics (QUICK) scheme proposed by Leonard [39] was applied to evaluate the face values used in the convection terms. This scheme is second order accurate and is considered highly conservative.

Given the grid of Figure 3.5, the face value of a quantity ϕ can be interpolated using the values at the centroids of the neighboring cells. The value at face f is given by the following 2nd order polynomial:

$$\phi_f = \phi_U + g_1(\phi_D - \phi_U) + g_2(\phi_U - \phi_{UU}) \tag{3.77}$$

$$g_1 = \frac{(x_f - x_U)(x_f - x_{UU})}{(x_D - x_U)(x_D - x_{UU})} \tag{3.78}$$

$$g_2 = \frac{(x_f - x_U)(x_D - x_f)}{(x_U - x_{UU})(x_D - x_{UU})} \tag{3.79}$$

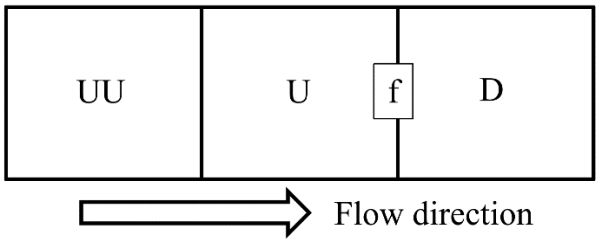

Figure 3.5: Computational stencil of QUICK scheme, from Tian [10].

where the subscripts f, D, U, UU stand for the current face, the downstream, the first upstream and the second upstream cells. However, the QUICK scheme is dispersive for large gradients. Therefore a flux limiter by Woodfield [40] was adopted. The flux limiter is a blending function between the first order upwind scheme and a higher order scheme and is defined as:

$$a(\eta) = \begin{cases} 0, & \eta < 0 \\ \dfrac{\eta}{\delta_f}, & 0 < \eta < \delta_f \\ 1, & \delta_f < \eta < 1 - \delta_f \\ 1 - \dfrac{\eta}{\delta_f}, & 1 - \delta_f < \eta < 1 \\ 0, & \eta > 1 \end{cases} \tag{3.80}$$

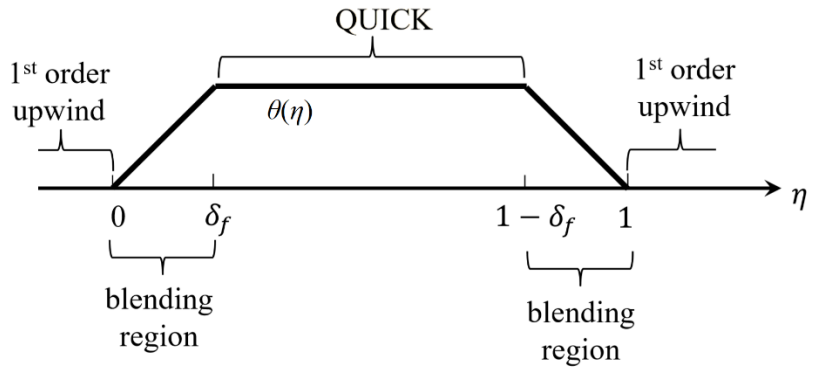

Figure 3.6: Schematic figure of flux limiter by Woodfield [40].

where, δ_f indicates the size of the blending region between the first order upwind and the QUICK. Tian [10] did some numerical tests and found that $\delta_f = 0.1$ works best for VISVE.

$$\eta = \frac{\phi_U - min(\phi_{UU}, \phi_D)}{|\phi_{UU} - \phi_D|} \tag{3.81}$$

Then, the QUICK scheme is modified to the following formulation:

$$\phi = \phi_U + a(\eta)[g_1(\phi_D - \phi_U) + g_2(\phi_U - \phi_{UU})] \tag{3.82}$$

Chapter 4: 2-D Hydrofoils in Cavitating Conditions

4.1 GRID CONFIGURATION

The following results are for a NACA66 hydrofoil with 4% thickness to chord length ratio and 1% camber to chord length ratio. The grid configuration in VISVE and RANS are shown in Figure 4.1 and Figure 4.2, respectively. The VISVE domain is much more compact with 26,000 cells compared to the 167,000 cells of the RANS domain. In the RANS model, the cavitation was modeled as steady laminar flow, whereas in VISVE the flow was modeled as unsteady with $\Delta t = 0.0001\ s$.

The commercial software ANSYS-FLUENT [41] was used for the RANS cases. PRESTO!, was used for the pressure face interpolation and QUICK for the momentum and vapor transport equations. The gradients were calculated using the Least-squares-cell-based scheme. The input values for the simulations were:

- Foil length: $L = 0.04\ m$
- Inflow velocity: $U_\infty = 0.122\ {}^{m}/_{s}$
- Angle of Attack: $AOA = 4^o$
- Liquid viscosity: $\mu_l = 0.001\ {}^{kg}/_{m \cdot s}$
- Vapor viscosity: $\mu_v = 0.0000134\ {}^{kg}/_{m \cdot s}$
- Liquid density: $\rho_l = 998.2\ {}^{kg}/_{m^3}$
- Vapor density: $\rho_v = 0.5542\ {}^{kg}/_{m^3}$
- Zwart-Gerber-Belamri's bubble radius: $R_B = 10^{-5} m$

The Reynold number is $Re \approx 4800$, which corresponds to a laminar flow regime. In reality, cavitation occurs at much higher Reynolds numbers (e.g. $Re = 2 \times 10^6$) which correspond to turbulent flow regimes. Forcing cavitation for a laminar case results in

unrealistic values for the foil length, inflow velocity and vapor pressure. The cavitation phenomenon is quantified by the dimensionless variable, cavitation number:

$$\sigma = \frac{p - p_v}{\frac{1}{2}\rho_l {U_\infty}^2} \qquad (4.1)$$

Results for wetted and cavitating cases of $\sigma = 1.2$, $\sigma = 1.0$ and $\sigma = 0.8$ will be presented. The simulations were run on TACC Stampede node [42].

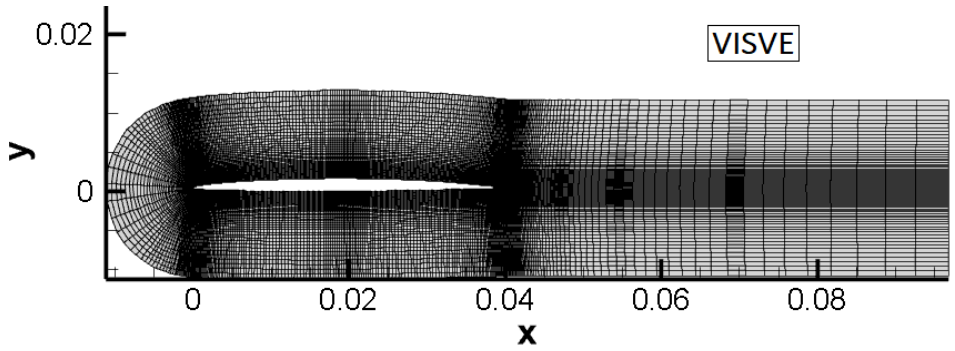

Figure 4.1: VISVE computation domain and grid configuration (26,000 cells)

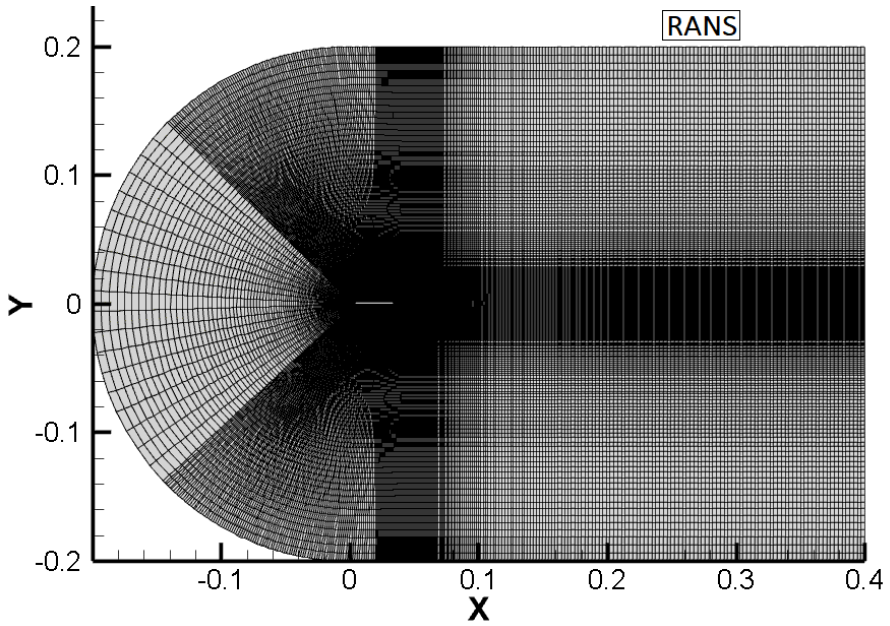

Figure 4.2: RANS computation domain and grid configuration (167,000 cells)

4.2 WETTED CASE

Since cavitation is a pressure-driven phenomenon, it is important to validate the pressure coefficient predicted from the wetted cases before we go into cavitating flow. To model wetted flow, a high cavitation number ($\sigma = 1.6$) was used. The comparison of pressure distribution predicted by VISVE and RANS is shown in Figure 4.3. Good correspondence between the two model validates the pressure calculation scheme in VISVE in wetted case.

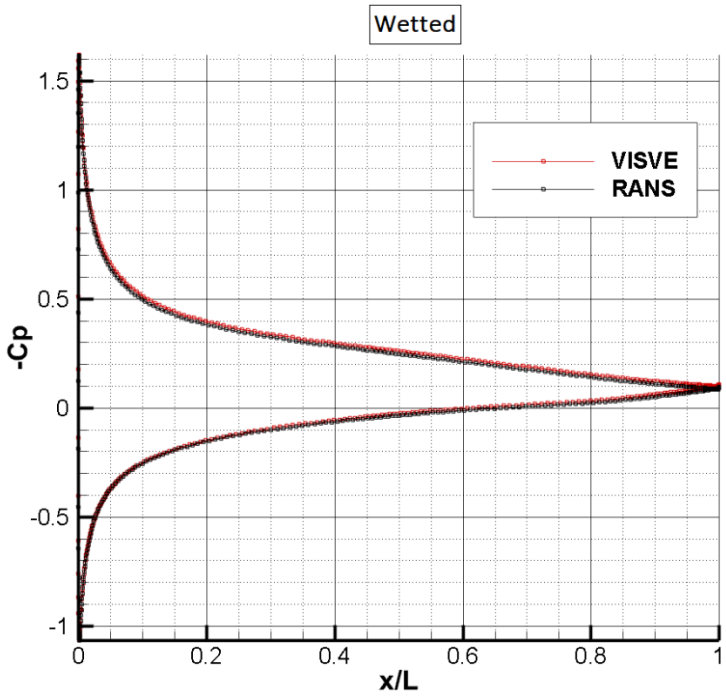

Figure 4.3: Comparison of pressure coefficient distribution on the hydrofoil predicted from VISVE and RANS $Re = 4{,}800, AOA = 4°$, wetted case

4.3 CAVITATION NUMBER =1.2

The cavitation number was set to $\sigma = 1.2$. The cavity shape predicted by VISVE and RANS is compared in Figure 4.4. Similarity can be observed in the cavity shape.

However, the cavity predicted by RANS has a slightly greater vapor volume fraction near the foil.

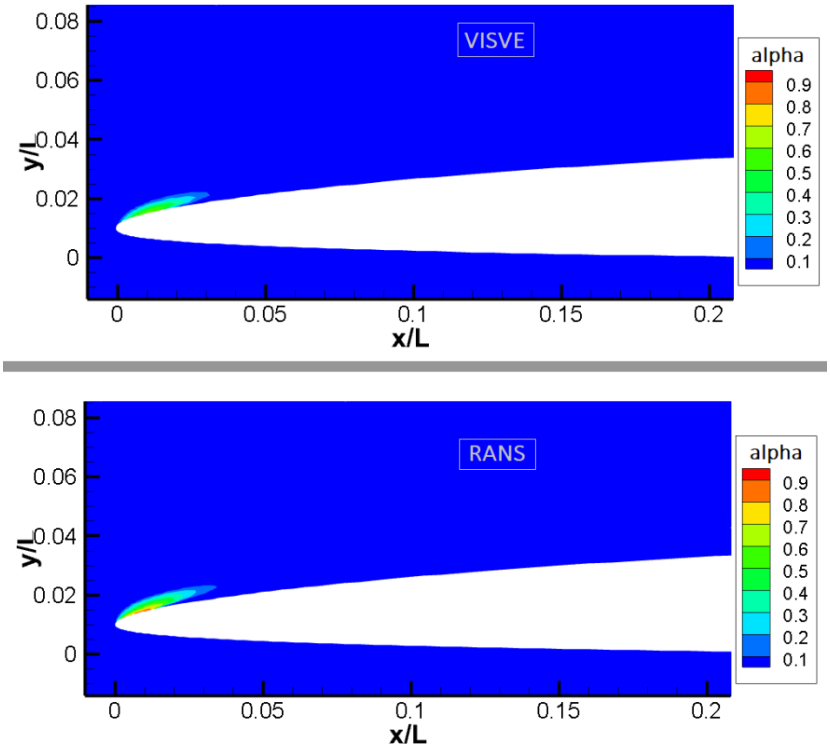

Figure 4.4: Comparison of cavity shape predicted by VISVE and RANS using Z-G-B cavitation model at $Re = 4{,}800, AOA = 4°, \sigma = 1.2$

Then the comparison of pressure coefficient distribution is presented in Figure 4.5. There is some discrepancy in the pressure coefficient behind the cavity, which will become more obvious for smaller cavitation numbers.

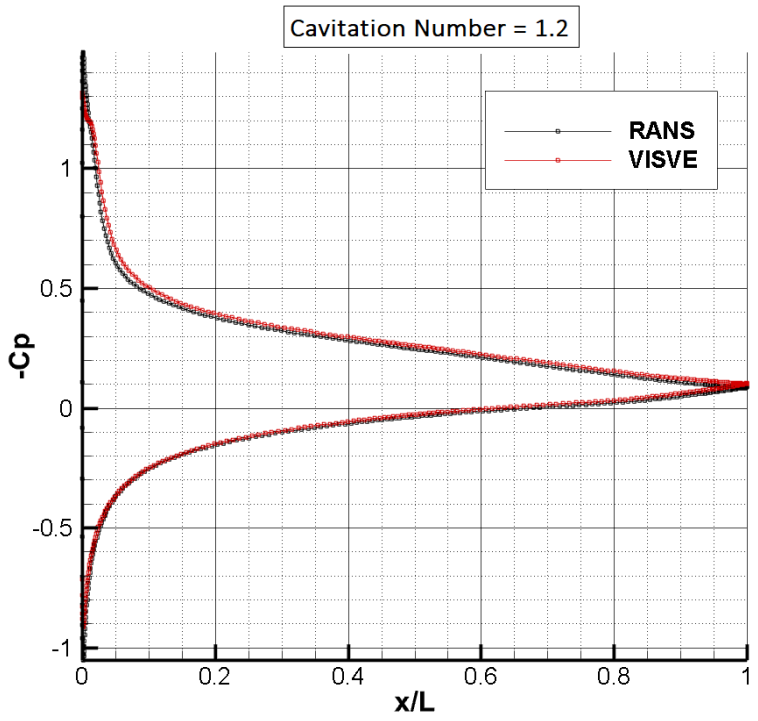

Figure 4.5: Comparison of pressure coefficient distribution on the hydrofoil predicted from VISVE and RANS using Z-G-B cavitation model $Re = 4{,}800, AOA = 4°, \sigma = 1.2$

4.4 CAVITATION NUMBER =1.0

The cavitation number was then lowered to $\sigma = 1.0$. The comparison of cavity shape and pressure coefficient distribution on the hydrofoil surface is presented in Figure 4.6 and Figure 4.7, respectively. The cavity length obtained from the two models agrees well with each other, which is about 5% chord length. Again, there is a difference in the pressure coefficient behind the cavity.

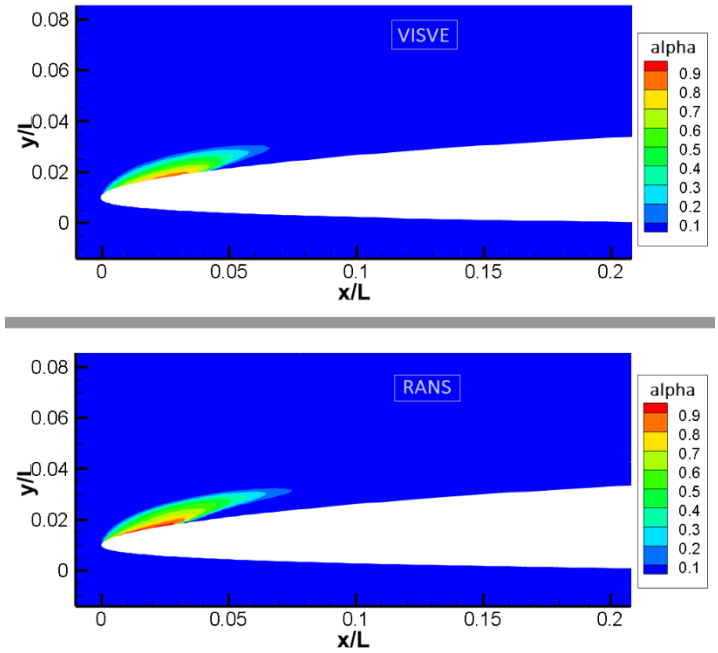

Figure 4.6: Comparison of cavity shape predicted by VISVE and RANS using Z-G-B cavitation model at $Re = 4{,}800, AOA = 4°, \sigma = 1.0$

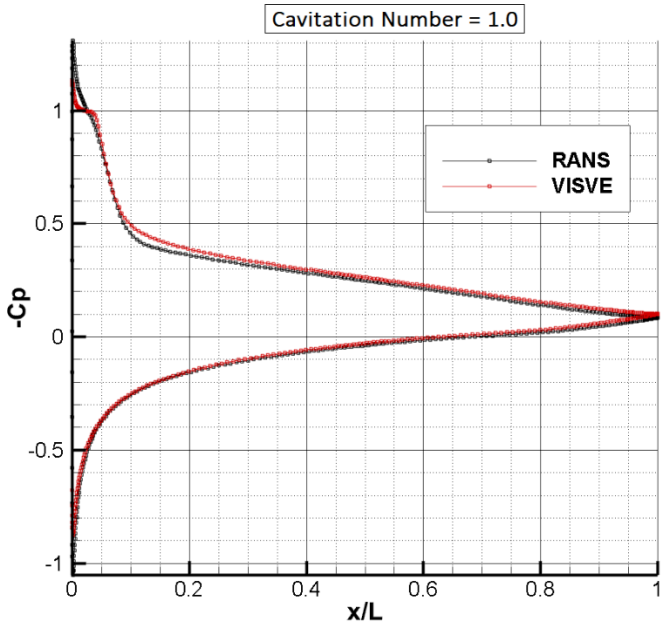

Figure 4.7: Comparison of pressure coefficient distribution on the hydrofoil predicted from VISVE and RANS using Z-G-B cavitation model $Re = 4{,}800, AOA = 4°, \sigma = 1.0$

4.5 CAVITATION NUMBER =0.8

Then, the cavitation number was further lowered to 0.8. In this case, RANS has a slightly longer cavity with the tail of the cavity extending to 20% the chord length. The main difference, however, is in the pressure distribution. The pressure behind the cavity is very different, possibly due to the fact that the baroclinic torque P_ω and the residual viscous terms Q_ω are neglected.

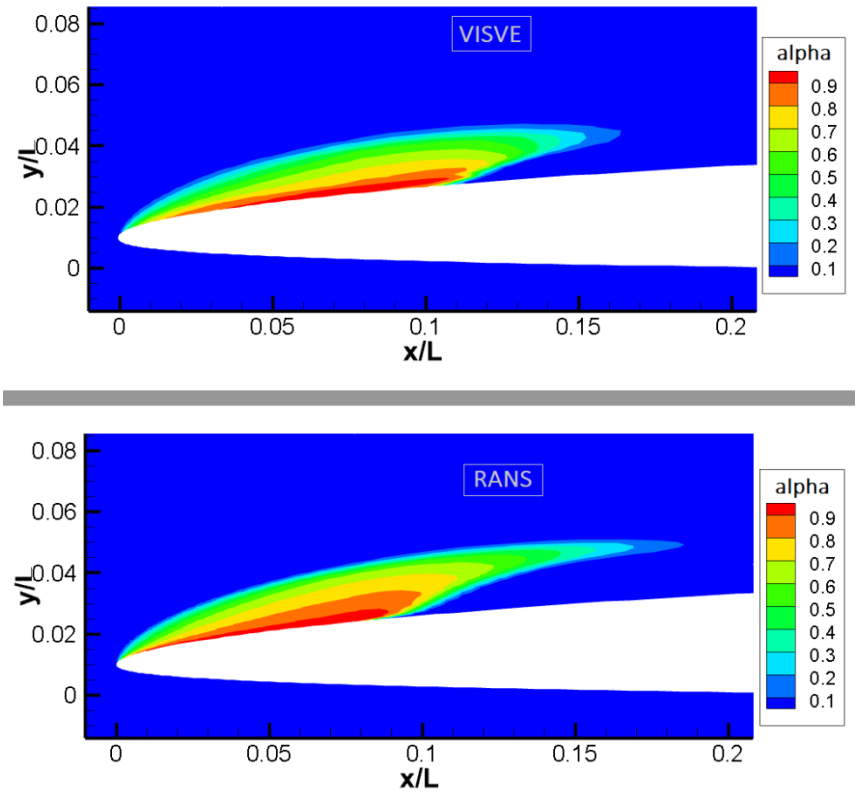

Figure 4.8: Comparison of cavity shape predicted by VISVE and RANS using Z-G-B cavitation model at $Re = 4{,}800, AOA = 4°, \sigma = 0.8$

At this point, it is worth noting that the pressure distribution is not constant underneath the cavity. Indeed, cavitation models based on the Rayleigh-Plesset equation require pressures lower than vapor pressure for cavitation inception to occur (Appendix E).

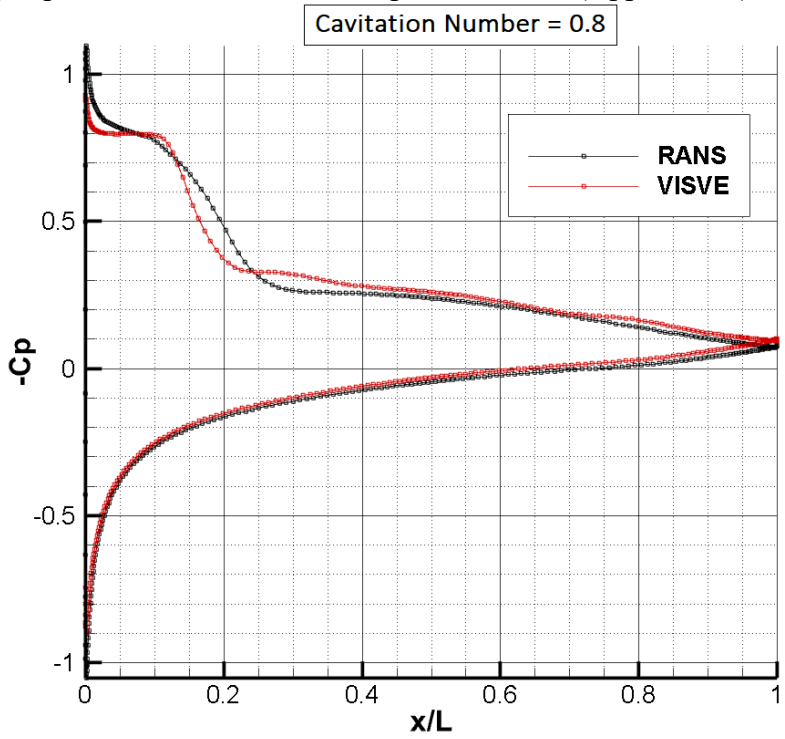

Figure 4.9: Comparison of pressure coefficient distribution on the hydrofoil predicted from VISVE and RANS using Z-G-B cavitation model $Re = 4{,}800, AOA = 4°, \sigma = 0.8$

For this cavitation number alone, some additional results for Re $= 2500$ are included. Similar to the previous figures, the following results compare the pressure and cavity of VISVE and RANS. It is obvious that the viscosity affects the size of the cavity, with more viscous flows related to smaller cavities. Again, VISVE seems to under predict the maximum vapor volume fraction, resulting in a much smaller cavity. This difference can be clearly seen in the pressure distribution.

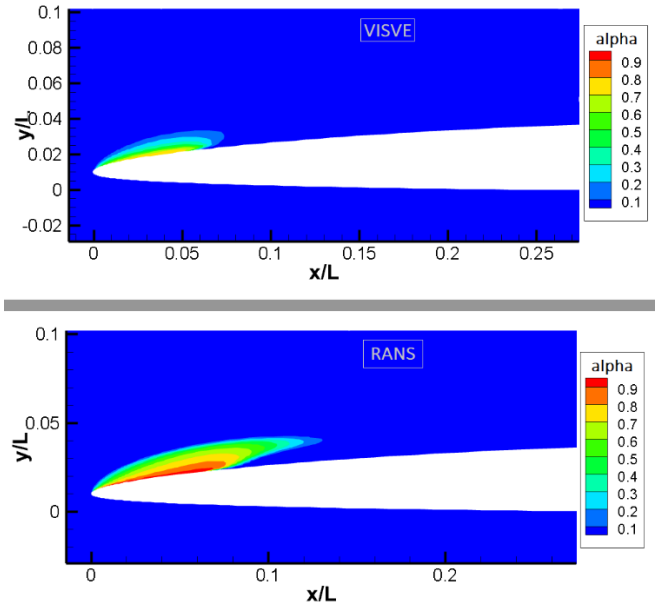

Figure 4.10: Comparison of pressure coefficient distribution on the hydrofoil predicted from VISVE and RANS using Z-G-B cavitation model $Re = 2{,}500, AOA = 4°, \sigma = 0.8$

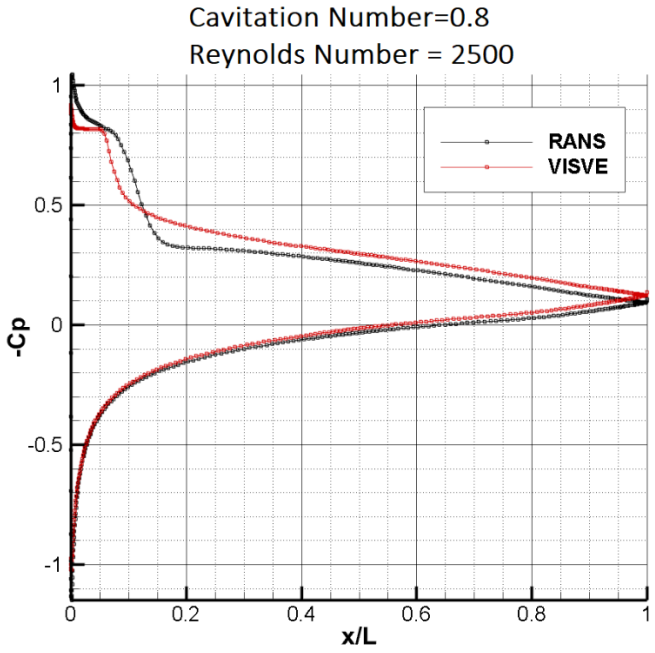

Figure 4.11: Comparison of pressure coefficient distribution on the hydrofoil predicted from VISVE and RANS using Z-G-B cavitation model $Re = 2{,}500, AOA = 4°, \sigma = 0.8$

5.6 CONVERGENCE STUDY

In order to validate the grid and time step independence of VISVE cavitation model, different sizes and different number of elements both on the surface of the hydrofoil and on the direction normal to the hydrofoil surface as well as different time steps have been applied to the 2-D VISVE model to predict the flow around the hydrofoil in cavitating conditions. Six cases are designed as shown in Table 4.1

Case No.	**1**	**2**	**3**	**4**	**5**	**6**
No. of Elements on foil	387	387	195	195	195	195
No. of Layer of cells	50	61	50	50	61	50
First layer height $[h/L]$[7]	$1 \cdot 10^{-3}$	$5 \cdot 10^{-4}$	$1 \cdot 10^{-3}$	$1 \cdot 10^{-3}$	$5 \cdot 10^{-4}$	$1 \cdot 10^{-3}$
Expansion ratio in Block I	1.06	1.06	1.06	1.06	1.06	1.06
No. of Elements on the wake	65	65	57	65	57	57
Expansion ratio in Block II	1.08	1.08	1.08	1.08	1.08	1.08
Time step size	$1 \cdot 10^{-4}$	$1 \cdot 10^{-4}$	$1 \cdot 10^{-4}$	$1 \cdot 10^{-4}$	$1 \cdot 10^{-4}$	$5 \cdot 10^{-5}$

Table 4.1 Cases setting for grid and time step independence study

The pressure distribution for different grid configuration and time step settings is presented in Figure 4.10. Satisfactory convergence results can be observed.

[7] The height, h, is made non-dimensional with the chord length, L.

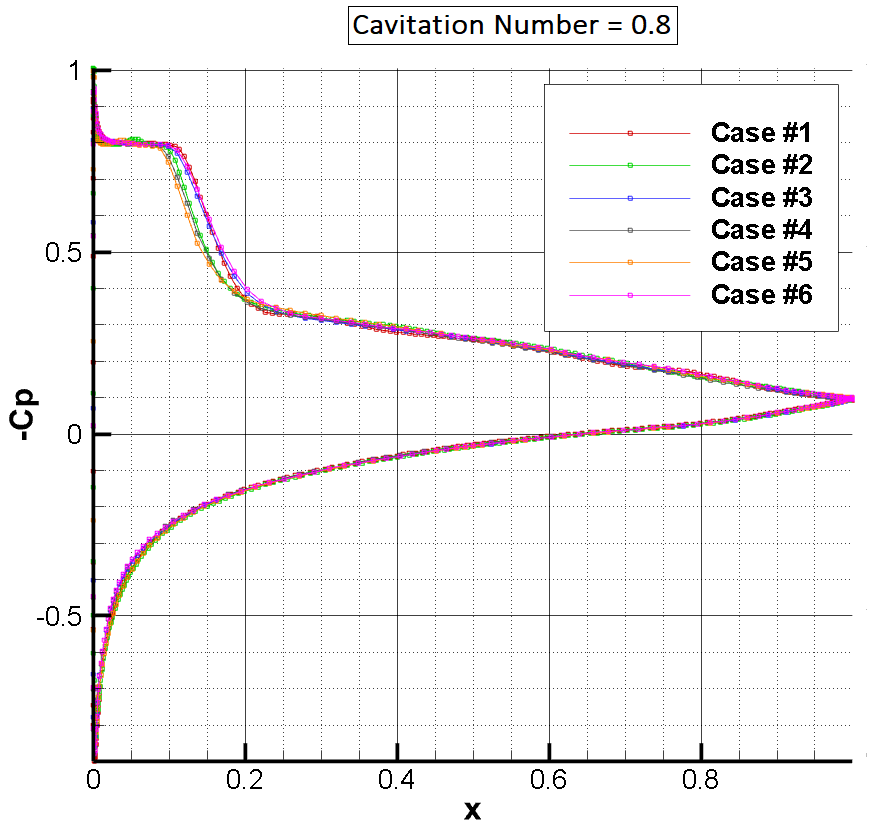

Figure 4.12: Pressure coefficient distribution for different cases at σ

Chapter 5: Conclusions and Future work

5.1 CONCLUSIONS

The VISVE method takes advantage of the spatial concentration of the vorticity and has proven to be more computationally efficient than RANS solver in the case of incompressible/wetted flow. The computational efficiency was not the objective of this thesis, hence the lack of computational time results. Nevertheless, it is the author's belief that there is great room for improvement for the VISVE/DIVE method, considering the fact that the computational domain of divergence and vapor transport equations may be limited in an area close to the cavity. A fully optimized VISVE method can be an efficient tool for the design and performance analysis of propellers and hydrofoils.

The main contribution of this study is that 2-D VISVE model has been extended to cavitating flow around hydrofoils. The results were promising but more adjustments need to be made in order to achieve a more robust solver.

For cavitating flow, the general solving algorithm of VISVE was modified. Several major changes were made.

1. Vorticity equation was written in a more general form to include the change of density and dynamic viscosity due to the generation and collapse of the cavitating bubbles. Additional terms were added to the vorticity equation solver, correspondingly.
2. Divergence of velocity equation, governing the dynamics of local expansion/contraction rate, allowing the VISVE method to handle compressible flows. The strong coupling of the divergence and continuity equation via the pressure term was addressed using the SIMPLEC method.

3. Mixture model, which offers a vapor transport equation, was coupled with vorticity equation to model the condensation and evaporation process. The cavitating flow was treated as a homogeneous mixture of liquid and water vapor with varying density and dynamic viscosity. The two phases were both treated as incompressible flow.
4. Two cavitation models based on the simplified version of Rayleigh-Plesset equation were introduced into the VISVE model. Only the results from Zwart-Gerber-Belamri's model were presented in this thesis.

The extension of the 2-D VISVE model to cavitating applications allows the VISVE model to predict more complex flow phenomenon in the process of propeller/hydrofoil design and performance analysis. This is part of a larger project with the goal being the accurate simulation of flow around 3-D hydrofoils and propellers in cavitating conditions based on 3-D VISVE method.

5.2 FUTURE WORK

5.2.1 VISVE

It is important to address the problems of the current formulation before moving on to turbulent or 3-D flows. One of the main issues is the pressure spike at the leading edge which is the main cause of instabilities in the codes. Additionally, in order to capture the full cavitation phenomenon, the baroclinic torque and the Q_ω terms need to be added in the code.

5.2.2 Turbulence Model

The current VISVE model includes only the laminar flow model, which limits the prediction at high Reynolds number. In order to overcome the limitation, turbulence models which offer the eddy viscosity could be developed. As an initial study, Hao and Kinnas [8] in OEG worked on extracting the turbulent viscosity from a RANS model adding it to the molecular viscosity in the current 2-D laminar VISVE scheme. Specifically, a coupling scheme between VISVE and OpenFOAM was developed via Shared Memory or MPI. OpenFOAM provides the turbulent viscosity based on the vast turbulent models embedded in the library; while VISVE provides the mean velocity needed in the turbulent models.

Another way to include turbulent effects is to add solvers the needed in turbulent models in VISVE itself and then replace the molecular viscosity by the eddy viscosity. Ms You in the OEG is currently working on implementing turbulence models into the VISVE solver.

5.2.3 3D VISVE

In three-dimensional cases, the vorticity- velocity solver is much more complicated than that in the 2-D case for several reasons. Firstly, vorticity will appear as a vector instead of a scalar. Secondly, the vortex stretching term needs to be added into the vorticity equation, which significantly increases the complexity of the partial differential equation. Finally, the computational cost in 3-D is considered to be much higher than that in 2-D.

Though with all those difficulties in the way, Tian [10] and Wu et all [3,4] have conducted a considerable amount of investigation in 3-D VISVE and applied it to the prediction of flow around 3-D hydrofoils and propellers in both forward and backing conditions.

Next step will be adding turbulent flow effects as well as extending the current cavitation model in the case of 3-D hydrofoils and propellers.

5.2.4 Parallelization of the code

The VISVE model can be fully parallelized. Significant efforts have been devoted to the parallelization of 2-D and 3-D VISVE for wetted flow by Wu *et al* [2], which significantly improved the computational efficiency and the shortened the computational time. More work needs to be performed for the parallelization in case of cavitating flow.

Appendices

APPENDIX A

The momentum equations can be written in the following vector form:

$$\frac{\partial \vec{q}}{\partial t} + (\vec{q} \cdot \vec{\nabla})\vec{q} = -\frac{\vec{\nabla} p}{\rho} + \frac{1}{\rho}\,\vec{\nabla} \cdot \bar{\bar{T}} \tag{A.1}$$

where $\vec{q}$ is the velocity vector, p is the pressure, ρ is the density and $\bar{\bar{\mathrm{T}}}$ is the stress tensor. The constitutive relation for the isotropic stress tensor, is:

$$\bar{\bar{T}} := \tau_{ij} = 2\mu\, S_{ij} + \lambda\, S_{kk}\delta_{ij} \tag{A.2}$$

where $S_{ij} := \frac{1}{2}\left(\frac{\partial q_i}{\partial x_j} + \frac{\partial q_j}{\partial x_i}\right) = \frac{1}{2}\left[\vec{\nabla}\vec{q} + \left(\vec{\nabla}\vec{q}\right)^T\right]$ is the strain tensor, μ is the dynamic viscosity and λ is $Lame'$ constant. According to Stokes' assumption, the bulk modulus should be zero, $K := \lambda + \frac{2}{N}\mu = 0$, so for the 3-D problem $\lambda = -\frac{2}{3}\mu$ and for the 2-D problem $\lambda = -\mu$. Therefore, the stress tensor can be written in the following matrix form:

$$\bar{\bar{T}} = \mu\left[\vec{\nabla}\vec{q} + \left(\vec{\nabla}\vec{q}\right)^T\right] - I\,\frac{2}{N}\left[\mu(\vec{\nabla} \cdot \vec{q})\right] \tag{A.3}$$

where $\delta_{ij} = I$, is the the identity matrix. Using identity (D.1), the left-hand side of the momentum equation becomes:

$$\frac{\partial \vec{\mathrm{q}}}{\partial \mathrm{t}} + (\vec{\mathrm{q}} \cdot \vec{\nabla})\vec{\mathrm{q}} = \frac{\partial \vec{\mathrm{q}}}{\partial \mathrm{t}} + \vec{\nabla}\left(\frac{1}{2}\mathrm{q}^2\right) - \vec{\mathrm{q}} \times \vec{\omega} \tag{A.4}$$

Similarly, using identities (D.2) and (D.3) the right-hand side of the momentum equation becomes:

$$-\frac{\vec{\nabla}p}{\rho}+\frac{1}{\rho}\,\vec{\nabla}\cdot \mathrm{T}=$$

$$=-\frac{\vec{\nabla}p}{\rho}+\frac{1}{\rho}\vec{\nabla}\cdot\left[\,\mu\,\left(\vec{\nabla}\vec{q}+\left(\vec{\nabla}\vec{q}\right)^{T}\right)-I\,\frac{2}{N}\,\mu\left(\vec{\nabla}\cdot\vec{q}\right)\right]=$$

$$=-\frac{\vec{\nabla}p}{\rho}+\nu\vec{\nabla}\left(\vec{\nabla}\cdot\vec{q}\right)+\nu\nabla^{2}\vec{q}+\frac{\vec{\nabla}\mu}{\rho}\cdot\left(\vec{\nabla}\vec{q}+\left(\vec{\nabla}\vec{q}\right)^{T}\right)-\frac{2}{N\rho}\vec{\nabla}\left(\mu\,\vec{\nabla}\cdot\vec{q}\right)=$$

$$=-\frac{\vec{\nabla}p}{\rho}+\nu\vec{\nabla}\left(\vec{\nabla}\cdot\vec{q}\right)+\nu\left(\vec{\nabla}\left(\vec{\nabla}\cdot\vec{q}\right)-\vec{\nabla}\times\vec{\omega}\right)+2\,\frac{\left(\vec{\nabla}\mu\cdot\vec{\nabla}\right)\vec{q}}{\rho}+\frac{1}{\rho}\vec{\nabla}\mu\times\vec{\omega}$$

$$-\frac{2}{N\rho}\left[\nabla\mu\left(\vec{\nabla}\cdot\vec{q}\right)+\mu\vec{\nabla}\left(\vec{\nabla}\cdot\vec{q}\right)\right] \qquad \text{(A.5)}$$

Combining relations (A.4) and (A.5) we get the following momentum equation:

$$\frac{\partial\vec{q}}{\partial t}+\vec{\nabla}\left(\frac{1}{2}q^{2}\right)-\vec{q}\times\vec{\omega}=-\frac{\vec{\nabla}p}{\rho}+\nu\vec{\nabla}\left(\vec{\nabla}\cdot\vec{q}\right)+\nu\left(\vec{\nabla}\left(\vec{\nabla}\cdot\vec{q}\right)-\vec{\nabla}\times\vec{\omega}\right)$$

$$+2\,\frac{\left(\vec{\nabla}\mu\cdot\vec{\nabla}\right)\vec{q}}{\rho}+\frac{1}{\rho}\vec{\nabla}\mu\times\vec{\omega}-\frac{2}{N\rho}\left[\vec{\nabla}\mu\left(\vec{\nabla}\cdot\vec{q}\right)+\mu\vec{\nabla}\left(\vec{\nabla}\cdot\vec{q}\right)\right] \qquad \text{(A.6)}$$

Finally, we take the dot product of the momentum equation with an arbitrary vector $\vec{n}$ (e.g. perpendicular or tangent to the foil) and solve for the pressure gradient

$$\frac{1}{\rho}\frac{\partial p}{\partial n}=\;-\frac{\partial q_{n}}{\partial t}-\frac{\partial}{\partial n}\left(\frac{1}{2}q^{2}\right)+\left(\vec{q}\times\vec{\omega}\right)\cdot\vec{n}+\nu\left(2\,\frac{\partial}{\partial n}\left(\vec{\nabla}\cdot\vec{q}\right)-\left(\vec{\nabla}\times\vec{\omega}\right)\cdot\vec{n}\right)$$

$$+2\,\frac{\left(\vec{\nabla}\mu\cdot\vec{\nabla}\right)q_{n}}{\rho}+\frac{1}{\rho}\left(\vec{\nabla}\mu\times\vec{\omega}\right)\cdot\vec{n}-\frac{2}{N\rho}\left[\frac{\partial\mu}{\partial n}\left(\vec{\nabla}\cdot\vec{q}\right)+\mu\,\frac{\partial}{\partial n}\left(\vec{\nabla}\cdot\vec{q}\right)\right] \qquad \text{(A.7)}$$

In the case of a 2-D problem the pressure equation (A.7) becomes:

$$\frac{\partial p}{\partial n}=-\rho\frac{\partial q_{n}}{\partial t}-\rho\,\frac{\partial}{\partial n}\left(\frac{1}{2}q^{2}\right)+\rho\,\left(\vec{n}\times\vec{q}\right)\cdot\vec{\omega}+\left(\vec{\mathrm{n}}\times\vec{\nabla}\mu\right)\cdot\vec{\omega}$$

$$+\mu\left(\frac{\partial}{\partial n}\left(\vec{\nabla}\cdot\vec{q}\right)-\left(\vec{\nabla}\times\vec{\omega}\right)\cdot\vec{n}\right)+2\,\vec{\nabla}\mu\cdot\vec{\nabla}q_{n}-\frac{\partial\mu}{\partial n}\left(\vec{\nabla}\cdot\vec{q}\right) \qquad \text{(A.8)}$$

APPENDIX B

In this appendix, we prove the relation for the viscous terms in the vorticity and divergence equation. The constitutive relation, (A.3), for the stress tensor, expresses the stress tensor, $\bar{\bar{T}}$, with respect to the strain tensor, $\bar{\bar{S}}$:

$$\bar{\bar{T}} = \mu\,\bar{\bar{S}} = \mu\left[\vec{\nabla}\vec{q} + \left(\vec{\nabla}\vec{q}\right)^{T} - \frac{2}{N} I\,\vec{\nabla}\cdot\vec{q}\right] \tag{B.1}$$

Substituting the stress tensor in the viscous torque term of the vorticity equation we get:

$$\begin{aligned}
&\vec{\nabla}\times\left[\tfrac{1}{\rho}\,\vec{\nabla}\cdot\bar{\bar{T}}\right] = \vec{\nabla}\times\left[\tfrac{1}{\rho}\,\vec{\nabla}\cdot\left(\mu\,\bar{\bar{S}}\right)\right] \\
&= \varepsilon_{ijk}\frac{\partial}{\partial x_j}\left(\frac{1}{\rho}\frac{\partial}{\partial x_m}(\mu\,S_{mk})\right) = \varepsilon_{ijk}\frac{\partial}{\partial x_j}\left(\nu\frac{\partial S_{mk}}{\partial x_m} + \frac{1}{\rho}\frac{\partial \mu}{\partial x_m}S_{mk}\right) = \\
&= \varepsilon_{ijk}\frac{\partial}{\partial x_j}\left(\nu\frac{\partial S_{mk}}{\partial x_m}\right) + \varepsilon_{ijk}\frac{1}{\rho}\frac{\partial \mu}{\partial x_m}\frac{\partial S_{mk}}{\partial x_j} + \varepsilon_{ijk}\frac{\partial}{\partial x_j}\left(\frac{1}{\rho}\frac{\partial \mu}{\partial x_m}\right)S_{mk}
\end{aligned} \tag{B.2}$$

For the 2-D problem N=2, so the above relation becomes:

$$\vec{\nabla}\times\left[\frac{1}{\rho}\,\nabla\cdot\bar{\bar{T}}\right] = \nabla\times\left[\frac{1}{\rho}\,\vec{\nabla}\cdot\left(\mu\begin{bmatrix}u_x - v_y & v_x + u_y\\ v_x + u_y & v_y - u_x\end{bmatrix}\right)\right] =$$

$$\begin{aligned}
&= \vec{\nabla}\times\left(\nu\begin{bmatrix}\left(\vec{\nabla}\cdot\vec{q}\right)_x - \omega_y\\ \left(\vec{\nabla}\cdot\vec{q}\right)_y + \omega_x\end{bmatrix}\right) + \frac{\vec{\nabla}\mu}{\rho}\times\begin{bmatrix}\left(\vec{\nabla}\cdot\vec{q}\right)_x - \omega_y\\ \left(\vec{\nabla}\cdot\vec{q}\right)_y + \omega_x\end{bmatrix} \\
&\quad + \left[\left(\frac{\mu_y}{\rho}\right)_x + \left(\frac{\mu_x}{\rho}\right)_y\right]\left(v_y - u_x\right) + \left[\left(\frac{\mu_x}{\rho}\right)_x - \left(\frac{\mu_y}{\rho}\right)_y\right]\left(v_x + u_y\right)
\end{aligned} \tag{B.3}$$

where $\vec{\nabla}\cdot\vec{q} := u_x + v_y$ and $\omega := v_x - u_y$. Finally, we can separate the diffusion term from the rest of the viscous terms:

$$\begin{aligned}
\vec{\nabla}\times\left[\frac{1}{\rho}\,\vec{\nabla}\cdot\bar{\bar{T}}\right] &= \vec{\nabla}\cdot\left[\nu_m\vec{\nabla}\omega\right] + \left(\vec{\nabla}\nu_m + \frac{\vec{\nabla}\mu}{\rho}\right)\times\vec{\nabla}\left(\vec{\nabla}\cdot\vec{q}\right) + \left(\frac{\vec{\nabla}\mu}{\rho}\right)\cdot\vec{\nabla}\omega \\
&\quad + \left[\left(\frac{\mu_y}{\rho}\right)_x + \left(\frac{\mu_x}{\rho}\right)_y\right]\left(v_y - u_x\right) + \left[\left(\frac{\mu_x}{\rho}\right)_x - \left(\frac{\mu_y}{\rho}\right)_y\right]\left(v_x + u_y\right)
\end{aligned} \tag{B.4}$$

Similarly, substituting the stress tensor in the viscous term of the divergence equation we get:

$$\vec{\nabla}\cdot\left[\frac{1}{\rho}\,\vec{\nabla}\cdot\bar{\bar{T}}\right]=\vec{\nabla}\cdot\left[\frac{1}{\rho}\,\vec{\nabla}\cdot\left(\mu\,\bar{\bar{S}}\right)\right]$$

$$=\frac{\partial}{\partial x_k}\left(\frac{1}{\rho}\frac{\partial}{\partial x_m}\left(\mu\,S_{mk}\right)\right)=\frac{\partial}{\partial x_k}\left(\nu\frac{\partial S_{mk}}{\partial x_m}+\frac{1}{\rho}\frac{\partial\mu}{\partial x_m}S_{mk}\right)=$$

$$=\frac{\partial}{\partial x_k}\left(\nu\frac{\partial S_{mk}}{\partial x_m}\right)+\frac{1}{\rho}\frac{\partial\mu}{\partial x_m}\frac{\partial S_{mk}}{\partial x_k}+\frac{\partial}{\partial x_k}\left(\frac{1}{\rho}\frac{\partial\mu}{\partial x_m}\right)S_{mk} \tag{B.5}$$

For the 2-D problem N=2, so the above relation becomes:

$$\vec{\nabla}\cdot\left[\frac{1}{\rho}\,\vec{\nabla}\cdot\bar{\bar{T}}\right]=\vec{\nabla}\cdot\left[\frac{1}{\rho}\,\vec{\nabla}\cdot\left(\mu\begin{bmatrix}u_x-v_y & v_x+u_y\\ v_x+u_y & v_y-u_x\end{bmatrix}\right)\right]=$$

$$=\vec{\nabla}\cdot\left(\nu\begin{bmatrix}\left(\vec{\nabla}\cdot\vec{q}\right)_x-\omega_y\\ \left(\vec{\nabla}\cdot\vec{q}\right)_y+\omega_x\end{bmatrix}\right)+\frac{\vec{\nabla}\mu}{\rho}\cdot\begin{bmatrix}\left(\vec{\nabla}\cdot\vec{q}\right)_x-\omega_y\\ \left(\vec{\nabla}\cdot\vec{q}\right)_y+\omega_x\end{bmatrix}$$

$$+\left[\left(\frac{\mu_y}{\rho}\right)_x+\left(\frac{\mu_x}{\rho}\right)_y\right]\left(v_x+u_y\right)+\left[\left(\frac{\mu_x}{\rho}\right)_x-\left(\frac{\mu_y}{\rho}\right)_y\right]\left(u_x-v_y\right) \tag{B.6}$$

where $\vec{\nabla}\cdot\vec{q}:=u_x+v_y$ and $\omega:=v_x-u_y$

Finally, we can separate the diffusion term from the rest of the viscous terms:

$$\vec{\nabla}\cdot\left[\frac{1}{\rho}\,\vec{\nabla}\cdot\bar{\bar{T}}\right]=\vec{\nabla}\cdot\left[\nu\vec{\nabla}(\nabla\cdot\vec{q})\right]+\left(\frac{\vec{\nabla}\mu}{\rho}\right)\cdot\vec{\nabla}(\vec{\nabla}\cdot\vec{q})-\left(\vec{\nabla}\nu+\frac{\vec{\nabla}\mu}{\rho}\right)\times\vec{\nabla}\omega$$

$$+\left[\left(\frac{\mu_y}{\rho}\right)_x+\left(\frac{\mu_x}{\rho}\right)_y\right]\left(v_x+u_y\right)+\left[\left(\frac{\mu_x}{\rho}\right)_x-\left(\frac{\mu_y}{\rho}\right)_y\right]\left(u_x-v_y\right) \tag{B.7}$$

APPENDIX C

The divergence equation (3.40) of section 3.6, treats the convective terms from the momentum equation explicitly which leads to a diffusion equation for $\nabla \cdot \vec{q}$. The following analysis assumes a different first approximation of pressure p_0, which leads to an advection-diffusion type equation for $\nabla \cdot \vec{q}$.

Applying the divergence operator in equation (A.1) we get:

$$\frac{\partial(\vec{\nabla} \cdot \vec{q})}{\partial t} + \vec{\nabla} \cdot \left[(\vec{q} \cdot \vec{\nabla})\vec{q}\right] = -\vec{\nabla} \cdot \left(\frac{\vec{\nabla} p}{\rho}\right) + \vec{\nabla} \cdot \left(\frac{1}{\rho}\, \vec{\nabla} \cdot \bar{\bar{T}}\right) \tag{C.1}$$

The divergence of convection becomes:

$$\vec{\nabla} \cdot \left[(\vec{q} \cdot \vec{\nabla})\vec{q}\right] = \frac{\partial}{\partial x_i}\left(u_j \frac{\partial u_i}{\partial x_j}\right) = \frac{\partial u_j}{\partial x_i}\frac{\partial u_i}{\partial x_j} + u_j \frac{\partial}{\partial x_j}\left(\frac{\partial u_i}{\partial x_i}\right) = \vec{\nabla}\vec{q} : \vec{\nabla}\vec{q} + (\vec{q} \cdot \vec{\nabla})(\vec{\nabla} \cdot \vec{q}) \tag{C.2}$$

$$(\vec{q} \cdot \vec{\nabla})(\vec{\nabla} \cdot \vec{q}) = u_j \frac{\partial}{\partial x_j}\left(\frac{\partial u_i}{\partial x_i}\right) = \frac{\partial}{\partial x_j}\left(u_j \frac{\partial u_i}{\partial x_i}\right) - \frac{\partial u_i}{\partial x_i}\frac{\partial u_j}{\partial x_j} = \vec{\nabla} \cdot \left[\vec{q}\,(\vec{\nabla} \cdot \vec{q})\right] - (\vec{\nabla} \cdot \vec{q})^2 \tag{C.3}$$

Substituting equations (C.2) and (C.3) into (C.1) we get:

$$\frac{\partial(\vec{\nabla} \cdot \vec{q})}{\partial t} + \vec{\nabla} \cdot [\vec{q}\,(\nabla \cdot \vec{q})] - (\vec{\nabla} \cdot \vec{q})^2 - \vec{\nabla} \cdot \left[\nu \vec{\nabla}(\vec{\nabla} \cdot \vec{q})\right] = -\vec{\nabla} \cdot \left(\frac{\vec{\nabla} p}{\rho}\right) + Q_{\vec{\nabla} \cdot \vec{q}} - \vec{\nabla}\vec{q} : \vec{\nabla}\vec{q} \tag{C.4}$$

where $Q_{\vec{\nabla} \cdot \vec{q}}$ are the residual viscous terms defined in equation (3.42) and $\vec{\nabla}\vec{q} : \vec{\nabla}\vec{q} = u_x^2 + 2u_y v_x + v_y^2$, in the case of a 2-D cartesian coordinate system.

APPENDIX D

Below we prove five important vector identities:

$$\vec{q} \times \left(\vec{\nabla} \times \vec{q}\right) = \vec{\nabla}\left(\frac{1}{2} q^2\right) - \left(\vec{q} \cdot \vec{\nabla}\right)\vec{q} \tag{D.1}$$

Proof:

$$\varepsilon_{ijk} q_j \left(\varepsilon_{klm} \frac{\partial}{\partial x_l} q_m\right) = \varepsilon_{ijk}\varepsilon_{klm} q_j \frac{\partial q_m}{\partial x_l} = \left(\delta_{il}\delta_{jm} - \delta_{im}\delta_{jl}\right) q_j \frac{\partial q_m}{\partial x_l} = q_j \frac{\partial q_j}{\partial x_i} - q_j \frac{\partial q_i}{\partial x_j}$$

$$\vec{\nabla} \times \left(\vec{\nabla} \times \vec{q}\right) = \vec{\nabla}\left(\vec{\nabla} \cdot \vec{q}\right) - \nabla^2 \vec{q} \tag{D.2}$$

Proof:

$$\varepsilon_{ijk} \frac{\partial}{\partial x_j}\left(\varepsilon_{klm} \frac{\partial}{\partial x_l} q_m\right) = \left(\delta_{il}\delta_{jm} - \delta_{im}\delta_{jl}\right) \frac{\partial^2 q_m}{\partial x_j \partial x_l} = \frac{\partial}{\partial x_i}\left(\frac{\partial q_j}{\partial x_j}\right) - \frac{\partial^2 q_i}{\partial x_j^2}$$

$$\vec{\nabla}\mu \times \vec{\omega} = \vec{\nabla}\mu \cdot \left(\left(\vec{\nabla}\vec{q}\right)^T - \vec{\nabla}\vec{q}\right) \tag{D.3}$$

Proof:

$$\varepsilon_{ijk} \frac{\partial \mu}{\partial x_j}\left(\varepsilon_{klm} \frac{\partial q_m}{\partial x_l}\right) = \left(\delta_{il}\delta_{jm} - \delta_{im}\delta_{jl}\right) \frac{\partial \mu}{\partial x_j} \frac{\partial q_m}{\partial x_l} = \frac{\partial \mu}{\partial x_j}\left(\frac{\partial q_j}{\partial x_i} - \frac{\partial q_i}{\partial x_j}\right)$$

$$\vec{\nabla} \times (\vec{q} \times \vec{\omega}) = \left(\vec{\omega} \cdot \vec{\nabla}\right)\vec{q} + \vec{q}\left(\vec{\nabla} \cdot \vec{\omega}\right) - \vec{\nabla} \cdot (\vec{q} \otimes \vec{\omega}) \tag{D.4}$$

Proof:

$$\varepsilon_{ijk} \frac{\partial}{\partial x_j}(\varepsilon_{klm}\, q_l\, \omega_m) = \left(\delta_{il}\delta_{jm} - \delta_{im}\delta_{jl}\right) \frac{\partial (q_l\, \omega_m)}{\partial x_j} = \left(\frac{\partial q_i}{\partial x_j}\omega_j + q_i \frac{\partial \omega_j}{\partial x_j}\right) - \frac{\partial\left(q_j\, \omega_i\right)}{\partial x_j}$$

where $\vec{q} \otimes \vec{\omega} = q_j\, \omega_i$ is the tensor product for vectors $\vec{q}$ and $\vec{\omega}$

$$\vec{\nabla} \times \left(\vec{\nabla}\phi\right) = \vec{0} \tag{D.5}$$

Proof:

$$\varepsilon_{ijk} \frac{\partial}{\partial x_j}\left(\frac{\partial \phi}{\partial x_k}\right) = \varepsilon_{ijk} \frac{\partial^2 \phi}{\partial x_j \partial x_k} = \left(\frac{\partial^2 \phi}{\partial x_j \partial x_k} - \frac{\partial^2 \phi}{\partial x_k \partial x_j}\right)_i = 0$$

APPENDIX E

In the case of the barotropic model or potential flow solvers, the pressure never drops below the cavitating pressure. Therefore, the pressure distribution on the foil is equal to the vapor pressure underneath the cavity and the results are similar to the right figure shown below.

In the case of viscous cavitation models based on the Rayleigh-Plesset equation sources due to evaporation can only occur if the pressure is below the vapor pressure. This can be easily deduced from the continuity equation, $\vec{\nabla} \cdot \vec{q} = C\sqrt{p - p_v}$. Therefore, the pressure underneath the cavity and especially at the leading edge where the sources are significant, is lower than vapor pressure. This resulting pressure distribution looks like the right figure.

ANSYS-FLUENT performs a cosmetic cut-off of the pressure distribution (for $p \leq p_v$) in the post-processing of the results. The difference between the actual pressure distribution and the post processed results is shown below.

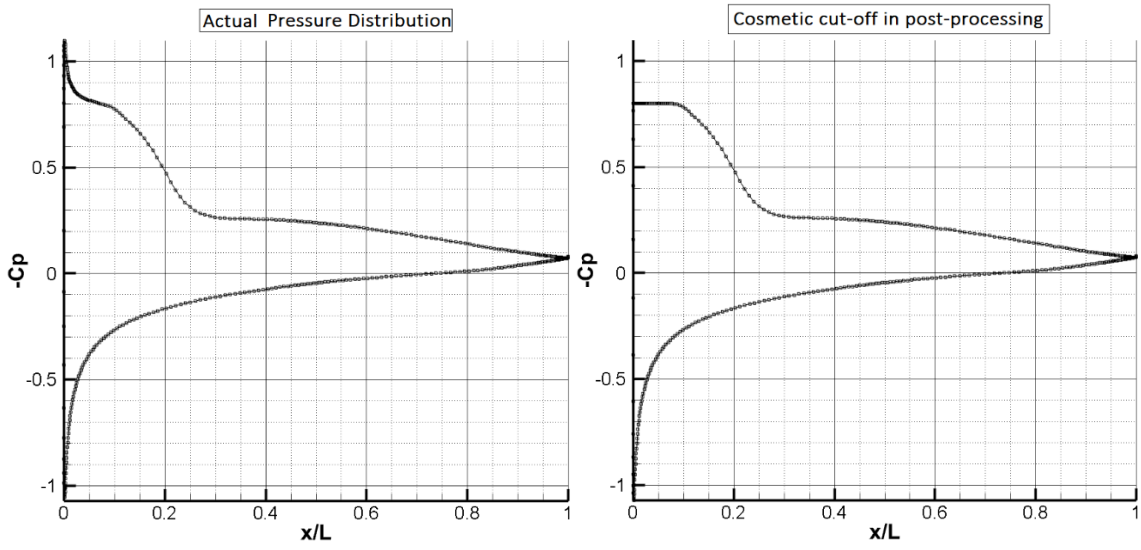

Figure E.1: Results from ANSYS -FLUENT for $\sigma = 0.8$ and $Re = 4800$ before and after post-processing.

References

1. Tian, Y., Kinnas, S.A.: A Viscous Vorticity Method for Propeller Tip Flows and Leading Edge Vortex. In: Symposium on Marine Propulsors (2015).

2. Wu, C., Xing, L., Kinnas, S.: A Viscous Vorticity Equation (VISVE) Method Applied to 2-D and 3-D Hyfrofoil in Both Forward and Backing Conditions. In: 23rd SNAME Symposium (2018).

3. Wu, C. and Kinnas, S.A., (2019) ``A Distributed Vorticity Model for Flow Past a 3-D Hydrofoil," 24th Offshore Symposium, SNAME (Society of Naval Architects and Marine Engineers), Houston, Texas, USA, February 20, 2019

4. Wu, C. and Kinnas, S.A., "A 3-D VIScous Vorticity Equation (VISVE) Method Applied to Flow Past a Hydrofoil of Elliptical Planform and a Propeller", 6th Symposium on Marine Propulsors, smp'19, May 26-30, 2019, Rome, Italy.

5. Wu, Y.: A Vorticity Based Model and its Application to Flow around an Impulsively Started Cylinder, MS thesis, Ocean Engineering Group, The University of Texas at Austin (2016).

6. Li, Z., Kinnas, S.A.: VISVE , a Vorticity Based Model Applied to Unidirectional and Alternating Flow around a Cylinder. In: 22th SNAME Sypothium (2017).

7. Li, Z.: VISVE , a Vorticity Based Model Applied to Unidirectional and Alternating Flow around a Cylinder, MS thesis, Ocean Engineering Group, The University of Texas at Austin (2017).

8. Hao Y., Kinnas, S.A.: Coupling Viscous Vorticity Equation (VISVE) Method with OpenFoam to Predict Turbulent Flow around 2-D Hydrofoils and Cylinders, MS thesis, Ocean Engineering Group, The University of Texas at Austin (2019).

9. Wu, C. and Kinnas, S.A., (2020) "Turbulent Flow Past a 3-D Hydrofoil Predicted by a Distributed Vorticity Method", Proceedings of the ASME 2020 39th International Conference on Ocean, Offshore and Arctic Engineering, OMAE2020,

June 28-July 3, 2020, Fort Lauderdale, FL, USA

10. Tian, Y.: Leading Edge Vortex Modeling and its Effect on Propulsor Performance, PhD dissertation, Ocean Engineering Group, The University of Texas at Austin, (2015).

11. Xing, L., "VISVE, a Vorticity Based Model Applied to 2-D Hydrofoils in Backing and Cavitating Conditions", MS thesis, Ocean Engineering Group, The University of Texas at Austin, May 2018.

12. Sauer, J., Schnerr, G.H.: Development of a New Cavitation Model based on Bubble Dynamics. ZAMM - J. Appl. Math. Mech. / Zeitschrift für Angew. Math. und Mech. 81, 561–562 (2001).

13. Zwart, P.J., Gerber, A.G., Belamri, T.: A Two-Phase Flow Model for Predicting Cavitation Dynamics. In: ICMF 2004 International Conference on Multiphase Flow (2004).

14. Koumoutsakos, G.-H.C. and P.D.: Vortex Methods and Vortex Motion, SIAM (1991).

15. Cottet, G.-H., Koumoutsakos, P.D.: Vortex Methods: Theory and Practice, Cambridge university press (2000).

16. Rosenhead, L.: The spread of vorticity in the wake behind a cylinder. Proc. R. Soc. London. Ser. A. 127, 590 LP-612 (1930)

17. Rosenhead, L.: The Formation of Vortices from a Surface of Discontinuity. Proc. R. Soc. A Math. Phys. Eng. Sci. 134, 170–192 (1931).

18. Krasny, R.: Desingularization of periodic vortex sheet roll-up. J. Comput. Phys. 65, 292–313 (1986).

19. Krasny, R.: A study of singularity formation in a vortex sheet by the point-vortex approximation. J. Fluid Mech. 167, 65–93 (1986).

20. Chorin, A.J.: Numerical study of slightly viscous flow. J. Fluid Mech. 57, 785–796 (1973).

21. Hald, O.H.: Convergence of Vortex Methods for Euler's Equations, III. SIAM J. Numer. Anal. 24, 538–582 (1987).

22. Beale J., Majda, a: Vortex Methods {I}: Convegence in Three Dimensions. Math. Comput. 39, 1–27 (1982).

23. Ogami, Y., Akamatsu, T.: Viscous flow simulation using the discrete vortex model—the diffusion velocity method. Comput. Fluids. 19, 433–441 (1991).

24. Koumoutsakos, P., Leonard, A., Pépin, F.: Boundary Conditions for Viscous Vortex Methods. J. Comput. Phys. 113, 52–61 (1994).

25. Barba, L. a: Vortex Method for computing high-Reynolds number Flows: Increased accuracy with a fully mesh-less formulation, PhD dissertation, California Institute of Technology (2004).

26. Leonard, A.: Vortex methods for flow simulation, J. Computat. Phys. 37.3, 289-335 (1980).

27. Anderson, C.R.: Vorticity boundary conditions and boundary vorticity generation for two-dimensional viscous incompressible flows. J. Comput. Phys. 80, 72–97 (1989).

28. Kinnas, S.A.: CAVITATION HOME PAGE at the University of Texas at Austin, http://cavity.caee.utexas.edu

29. Kinnas S.A., Fine N.E. (1991) Non-Linear Analysis of the Flow Around Partially or Super-Cavitating Hydrofoils by a Potential Based Panel Method. In: Morino L., Piva R. (eds) Boundary Integral Methods. Springer, Berlin, Heidelberg

30. Xu, Z., Kim, M., Lu, T., Oh, W., Glimm, J., Samulyak, R., Li, X., Tzanos, C.: Discrete Bubble Modeling of Unsteady Cavitating Flow. Int. J. Multiscale Comput.

Eng. 4, 601–616 (2006).

31. Tryggvason, G., Bunner, B., Esmaeeli, A., Juric, D., Al-Rawahi, N., Tauber, W., Han, J., Nas, S., Jan, Y.J.: A Front-Tracking Method for the Computations of Multiphase Flow. J. Comput. Phys. 169, 708–759 (2001).

32. Goncalv, E., Silva, D., Goncalv, E., Silva, D.: Numerical Simulation of Cavitating Flows with Homogeneous Models, Comput. Fluids. 38.9, 1682-1696 (2010).

33. Tsuda, S.: Development and Validation of Multi-process Cavitation Model. In: Proc. 8th International Symposium on Cavitation 978–981 (2012).

34. Gibou, F., Chen, L., Nguyen, D., Banerjee, S.: A level set based sharp interface method for the multiphase incompressible Navier–Stokes equations with phase change. J. Comput. Phys. 222, 536–555 (2007).

35. Plesset, M.S., Prosperetti, A.: Bubble dynamics and cavitation. Annu. Rev. Fluid Mech. 9, 145–185 (1977).

36. Oliver D. Kellogg: Foundations of Potential Theory. Dover Publications.

37. Joel H. Ferziger, Milovan Perić, Robert L. Street: Computational Methods for Fluid Dynamics. Springer (4th Edition).

38. Kinnas, S.A. VIScous Vorticity Equation (VISVE) for Turbulent 2-D Flows with Variable Density and Viscosity. J. Mar. Sci. Eng. 2020, 8, 191.

39. Leonard, B.P.: A stable and accurate convective modelling procedure based on quadratic upstream interpolation. Comput. Methods Appl. Mech. Eng. 19, 59–98 (1979).

40. Woodfield, P.L., Suzuki, K., Nakabe, K.: A simple strategy for constructing bounded convection schemes for unstructured grids. Int. J. Numer. Methods Fluids. 46, 1007–1024 (2004).

41. ANSYS, Inc.: Fluent User Guide and PDF Documentation for Release 17.1,

www.ansys.com/products/fluids/ansys-fluent

42. Center Texas Advanced Computing: Stampede User Guide, https://portal.tacc.utexas.edu/user-guides/stampede.